J. Fluid Mech. (2001), *vol.* 444, *pp.* 223–256. Printed in the United Kingdom

The cavitation instability induced by the development of a re-entrant jet

By MATHIEU CALLENAERE, JEAN-PIERRE FRANC, JEAN-MARIE MICHEL, AND MICHEL RIONDET

Laboratoire des Ecoulements Géophysiques et Industriels, BP 53, 38041 Grenoble Cedex 9, France

(Received 12 September 2000 and in revised form 5 March 2001)

The instability of a partial cavity induced by the development of a re-entrant jet is investigated on the basis of experiments conducted on a diverging step. Detailed visualizations of the cavity behaviour allowed us to identify the domain of the re-entrant jet instability which leads to classical cloud cavitation. The surrounding regimes are also investigated, in particular the special case of thin cavities which do not oscillate in length but surprisingly exhibit a re-entrant jet of periodical behaviour. The velocity of the re-entrant jet is measured from visualizations, in the case of both cloud cavitation and thin cavities. The limits of the domain of the re-entrant jet instability are corroborated by velocity fluctuation measurements. By varying the divergence and the confinement of the channel, it is shown that the extent of the auto-oscillation domain primarily depends upon the average adverse pressure gradient in the channel. This conclusion is corroborated by the determination of the pressure gradient on the basis of LDV measurements which shows a good correlation between the domain of the cloud cavitation instability and the region of high adverse pressure gradient. A simple phenomenological model of the development of the re-entrant jet in an adverse pressure gradient confirms the strong influence of the pressure gradient on the development of the re-entrant jet and particularly on its thickness. An ultrasonic technique is developed to measure the re-entrant jet thickness, which allowed us to compare it with the cavity thickness. By considering an estimate of the characteristic height of the perturbations developing on the interface of the cavity and of the re-entrant jet, it is shown that cloud cavitation requires negligible interaction between both interfaces, i.e. a thick enough cavity. In the case of thin cavities, this interaction becomes predominant; the cavity interface breaks at many points, giving birth to small-scale vapour structures unlike the large-scale clouds which are periodically shed in the case of cloud cavitation. The low-frequency content of the cloud cavitation instability is investigated using spectral analysis of wall pressure signals. It is shown that the characteristic frequency of cloud cavitation corresponds to a Strouhal number of about 0.2 whatever the operating conditions and the cavity length may be, provided the Strouhal number is computed on the basis of the maximum cavity length. For long enough cavities, another peak is observed in the spectra, at lower frequency, which is interpreted as a surge-type instability. The present investigations give insight into the instabilities that a partial cavity may undergo, and particularly the re-entrant jet instability. Two parameters are shown to be of most importance in the analysis of the re-entrant jet instability: the adverse pressure gradient and the cavity thickness compared to the re-entrant jet thickness. The present results allowed us to conduct a qualitative phenomenological analysis of the stability of partial cavities on cavitating hydrofoils. It is conjectured that cloud cavitation should occur for short enough cavities, of the order of half the chordlength, whereas the instability often observed

at the limit between partial cavitation and super-cavitation is here interpreted as a cavitation surge-type instability.

1. Introduction

Attached cavities are more or less unsteady and, in some cases, their length may undergo significant oscillations and they are considered unstable. The term cavitation instability is used for such situations in which no steady cavity actually exists. Cavitation instabilities are a subject of interest in the field of turbomachinery as they can induce abnormal dynamic behaviour, and also noise and erosion which are known as particularly serious for cloud cavitation.

We propose to distinguish, *a priori*, two main classes of instabilities for an attached cavity: intrinsic instabilities and system instabilities. This classification simply refers to the origin of the instability. If it originates in the cavity itself, the instability is of intrinsic type. If it is due to an interaction between the cavity and either other cavities (as in the case of a turbomachinery) or other components of the hydraulic system (such as inlet or outlet lines), it is system dependent.

Surge cavitation is a typical example of a system instability. It can be illustrated by a very simple one-dimensional model (Watanabe *et al.* 1998) of a cavity in a duct of given section A and inlet length L and of infinite outlet length for simplicity. If the cavity volume is defined by ϑ, the mass balance gives $Au = -\dot{\vartheta}$, where u is the velocity perturbation in the inlet duct. This equation simply expresses that the variations in cavity volume are balanced by the liquid flow rate. If no pressure perturbation is assumed at the inlet, the momentum balance gives $p = -\rho L\dot{u}$, where p is the pressure perturbation at the location of the cavity. By combining both relations, we get a second-order differential equation for the evolution of the pressure: $\rho LK\ddot{p} + Ap = 0$, where $K = -\mathrm{d}\vartheta/\mathrm{d}p$ is the classical cavitation compliance. It is generally positive as the cavity volume normally increases with a reduction of pressure. In such a case, the solution is periodic and the system is stable and auto-oscillates with the frequency $\omega = \sqrt{A/\rho LK}$. The physical reason for this stable behaviour is easy to understand. A decrease in pressure at the location of the cavity makes its volume increase. To counterbalance this, the flow decelerates in the inlet duct which makes the pressure at the cavity increase, due to the inertia of the inlet liquid column. Hence, the system is stable. From the above form of the oscillation frequency, it is clear that the dynamic behaviour of the cavity results from a coupling between the cavity itself, characterized here by its compliance, and the inlet duct, characterized by its length and area. Hence, it is typical of a system instability. On the other hand, the behaviour is actually unstable in the case of a negative cavitation compliance, as the equation for the pressure fluctuation clearly demonstrates that it does not oscillate but increases exponentially with time.

In the case of multiple cavities, as e.g. in the case of a turbomachinery with a cavity on each blade, the behaviour of a given cavity can be independent of the other ones or coupled with them according to the operating conditions. Rotating cavitation which is observed in inducers (Tsujimoto 1995) is a typical example of the latter case. Each cavity on each blade exhibits oscillations in volume (Hashimoto *et al.* 1996) which are coupled with the oscillations of the other cavities. In rotating cavitation, the cavitating region rotates faster than the impeller. These coherent oscillations of a system of multiple cavities is typical of cavitating cascades (Watanabe *et al.* 1999).

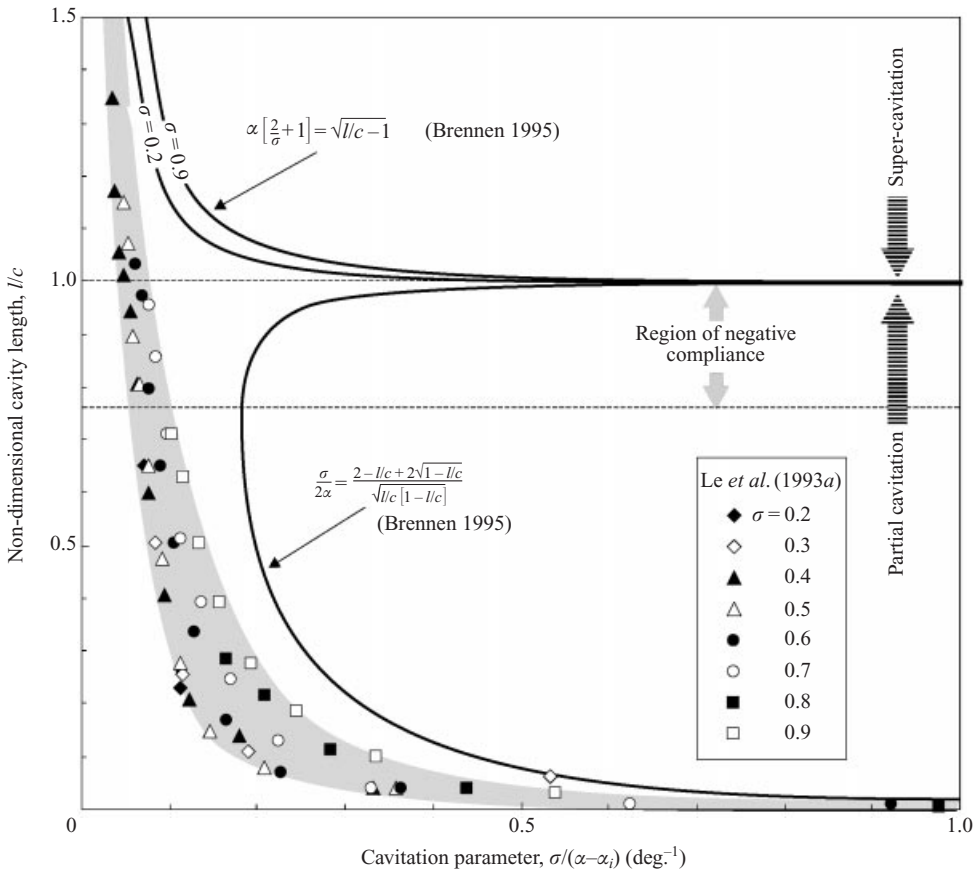

FIGURE 1. Typical variation of the cavity length l with the cavitation number σ. The cavity length l is made non-dimensional by the chord length c of the foil and the cavitation number is divided by the difference between the angle of attack α and the incipient angle of attack α_i. As a reference, the linear solution for a flat-plate hydrofoil (Brennen 1995) is shown in solid line.

In this sense, the instability of each cavity is not intrinsic but requires other cavities to develop. From the viewpoint of the turbomachinery as a whole, this instability is considered as local, unlike surge which is a global system instability involving the inlet and outlet lines (Tsujimoto 1995).

The dynamic behaviour of a cavity can also arise from its extreme sensitivity to external fluctuations. Figure 1 presents a typical variation of the cavity length with the cavitation number. The L-shape of the curve is classical. On the horizontal branch, i.e. for high enough values of the cavitation number σ or small enough partial cavities l, the cavity is almost insensitive to external pressure fluctuations. Conversely, on the vertical branch of the $l(\sigma)$ curve, the cavity behaves like an amplifier: small outer perturbations result in large-amplitude oscillations of the cavity. This extreme sensitivity to external perturbations occurs for long enough cavities. It is probably the origin of the oscillations sometimes observed at the transition between partial and supercavitation (see for instance Wade & Acosta 1966). This instability can still be considered as system dependent, in so far as it requires external perturbations to develop.

On the other hand, an intrinsic instability emanates from the cavity itself. The

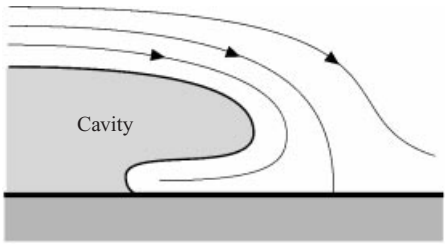

FIGURE 2. Schematic representation of the re-entrant jet flow in the closure region of an attached cavity.

development of a re-entrant jet at the back of the cavity and the subsequent oscillations of the cavity length is the most common type of intrinsic instability. Other types of intrinsic instabilities may exist as downstream travelling interface waves which have been predicted by computations (Watanabe *et al.* 1998) but not yet observed experimentally.

The principle of the re-entrant jet instability has been described by several researchers. Knapp, Daily & Hammitt (1970) give a rather precise description of the flow at the downstream end of a cavity. Closure of the cavity occurs where the external flow re-attaches to the wall (see figure 2). The flow which originally moves over the cavity has locally the structure of a liquid jet impinging obliquely upon the wall. The falling stream divides into two parts flowing parallel to the wall. One is the re-entrant jet which moves upstream causing cavity detachment. The other one makes the flow reattach to the wall. Moreover, if the interface of the cavity is considered as a streamline, a change of concavity would not be consistent with a minimum pressure inside the cavity, as can be seen from the normal projection of Euler equation. Hence, the development of a re-entrant jet at the downstream end of a cavity is a physical necessity.

However, it is clear that the re-entrant jet cannot exist continually, otherwise the cavity would be filled with liquid. Hence, we are led to suppose that periods of development of the re-entrant jet, which tend to fill the cavity, are followed by periods of emptying and entrainment of the two-phase mixture. This phenomenon is essentially controlled by inertia. A simple dimensional analysis leads to the conclusion that the oscillation frequency f is of the order of l/V_∞. Actually, the Strouhal number $S = fl/V_\infty$ of this instability, based on the maximum cavity length l was found to range between about 0.25 and 0.4 by many experimenters (see e.g. Kawanami, Kato & Yamaguchi 1998 for a comparison of results of various origins).

One of the pioneering works on the re-entrant jet instability is Furness & Hutton (1975). The dynamic behaviour of the cavity which develops on a Venturi-type nozzle is described and modelled by a two-dimensional unsteady potential flow theory. The early formation of the re-entrant jet is predicted well, together with the roller-type motion during the growth phase of the cavity. The computation stops when the re-entrant jet intersects the cavity interface and is unable to model the shedding of a cloud. More recently, a comparable work, carried out by de Lange (1996) (see also de Lange, de Bruin & van Wijngaarden 1994), gives a similar description of the break-off cycle for two-dimensional NACA foils. The generation mechanism of cloud cavitation was also investigated in detail by Kawanami *et al.* (1997). They had the simple but effective idea of putting an obstacle on the foil to stop the re-entrant jet and actually showed that it prevents the generation of cloud cavitation. Their

study definitely confirms the essential role of the re-entrant jet in the onset of cloud cavitation.

In 1989, Kubota *et al.* gave a detailed description of the flow structure around unsteady cloud cavitation on a stationary two-dimensional hydrofoil by laser Doppler anemometry using a conditional sampling technique. They showed that the shed cloud is a large-scale vortex structure containing many small cavitation bubbles. Yamaguchi *et al.* (1990) succeeded in measuring the micro-scale structure of the cavitation cloud using a laser holography system. They were able to quantify the bubble distribution as a function of their diameter. The pressure pulses induced by the collapse of those bubbles were measured by Le, Franc & Michel (1993*b*). Their pressure pulse height spectra confirm the well-known industrial observation that, from an erosion viewpoint, cloud cavitation is much more destructive than a stable sheet cavity. To reduce this, several possibilities were tested by Boehm, Stoffel & Ludwig (1997) and Boehm *et al.* (1998), including variations of the leading-edge geometry, air injection and the insertion of an obstacle to stop the re-entrant jet.

The structure of the two-phase flow inside the cavity was investigated by Stutz & Reboud (1997) and Reboud, Stutz & Coutier (1998) using a double optical probe. They succeeded in measuring the local void fraction and the velocity inside their cavities and showed that, for their cavitating conditions, the void fraction does not exceed 21%. Their velocity measurements also confirm the existence of a reversed two-phase flow along the wall. Other experimental techniques were used to investigate the structure of partial attached cavities, such as laser Doppler anemometry (Avellan & Dupont 1988; Dupont 1993), particle imaging velocimetry (Laberteaux & Ceccio 1998) and electrical impedance probes (George, Iyer & Ceccio 2000; Pham, Larrarte & Fruman 1998).

From a modelling viewpoint, beside the potential-based panel methods already mentioned (see also Dang & Kuiper 1998, 1999*a*, *b*), an effort was made to develop models able to describe not only the growth phase of the sheet cavity and the development of the re-entrant jet, but also the break-off and the fully detached cloud that a Lagrangian description of the cavity contour fails to predict. Several approaches were used to model the liquid–vapour mixture as a homogeneous fluid of variable density. Kubota (1988) and Kubota, Kato & Yamaguchi (1992) developed a local homogeneous model to describe the evolution of the bubble cluster and to compute the void fraction and so the density of the mixture. Reboud & Delannoy (1994) and Song & He (1998) used a somewhat arbitrary barotropic equation of state to describe the behaviour of the mixture. Furthermore, separated two-phase flow models are being developed using a free surface tracking method such as 'volume of fluid' to capture the interfaces (Dieval 1999; Dieval, Arnaud & Marcer 1998).

Most studies (including the present one) relate to two-dimensional configurations. However, three-dimensional effects may be important in the situation of a swept foil, for instance. De Lange (1996) has clearly shown that the re-entrant jet is reflected at an inclined cavity closure line and thus the jet velocity has a spanwise component. This feature can be explained by the conservation of the tangential momentum when the pressure gradient has no component in that direction. The whole behaviour of sheet cavitation on swept hydrofoils and in particular unsteadiness is affected by this three-dimensional effect as shown by Laberteaux & Ceccio (1998) and Duttweiler & Brennen (1998). Even in the case of two-dimensional experiments, it is often observed that the closure line of the sheet cavity has a convex shape (see for instance figure 9) and, thus, three-dimensional effects can be suspected, as mentioned by de Lange (1996).

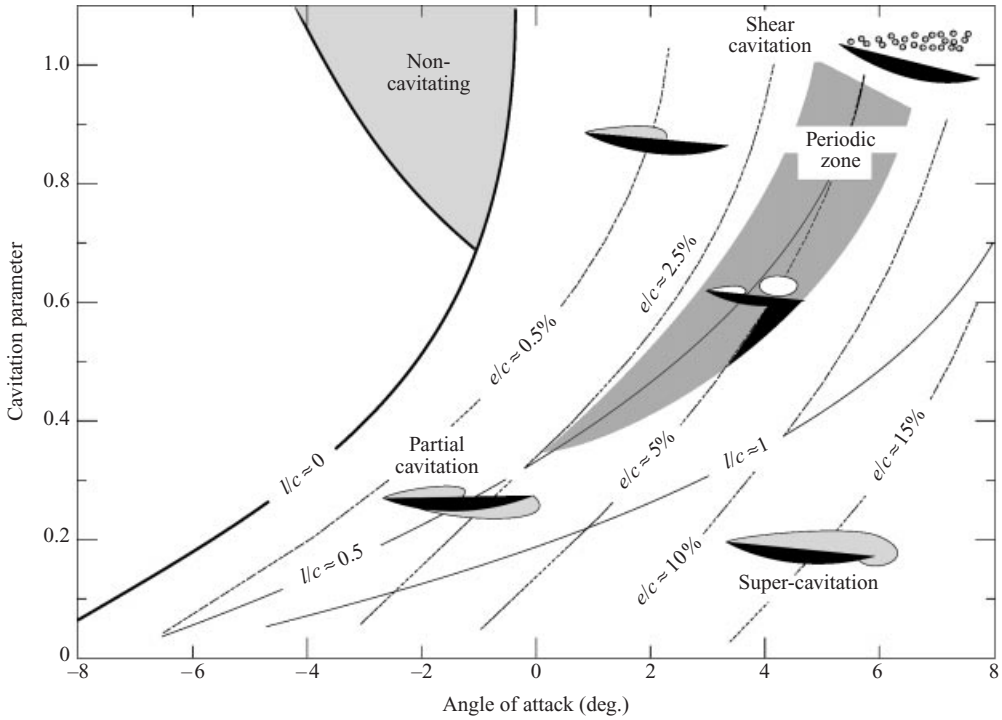

FIGURE 3. Cavitation patterns on the upper side of a plano-convex hydrofoil (after Le *et al.* 1993*a*). The periodic zone corresponds to the presence of a re-entrant jet and the develoment of cloud cavitation. l/c and e/c are the cavity length and the cavity thickness, non-dimensionalized by the chord length. In the case of cavity pulsations, l is the maximum cavity length.

Le, Franc & Michel (1993*a*) gave a comprehensive description of the global behaviour of partial cavities which develop on the flat side of a plano-convex hydrofoil. They noticed that cavity auto-pulsations occur in a limited domain of angle of attack and cavitation parameter. The region of cloud cavitation instability was found to be roughly centred on the curve $l/c = 0.5$, where c is cord length, as shown on figure 3. The photograph presented in figure 4 confirms that the instability occurs for relatively short cavities. All research workers do not reach the same conclusion, however. In their early work on a foil of similar shape, Wade & Acosta (1966) observed oscillations in cavity length and hydrodynamic forces when the cavity exceeds about 60% of the chord. They report that oscillations persist until the cavity is at least 120% of the chord. More recently, Tsujimoto (1995) also found that the region of instability is roughly centred on the curve $l/c = 1$ and thus that the instability occurs at the transition between partial and super-cavitation. Brennen (1995) and Tsujimoto (1995) argue that the flow is unstable in this region because the cavitation compliance is negative there, as can be seen on figure 1. However, we can wonder whether this negative cavitation compliance is not a mathematical artefact at the transition between partial and super-cavitation as the experimental curve $l(\sigma)$ does not exhibit any special features in this region. We see that a few fundamental questions concerning the re-entrant jet instability and its occurrence still need to be clarified. Among these questions, we can also mention the likely influence of the shape of the hydrofoil and of the corresponding pressure distribution on the onset of the instability. The thickness of the cavity may also be an important factor as Le *et al.* (1993*a*) suggest that friction

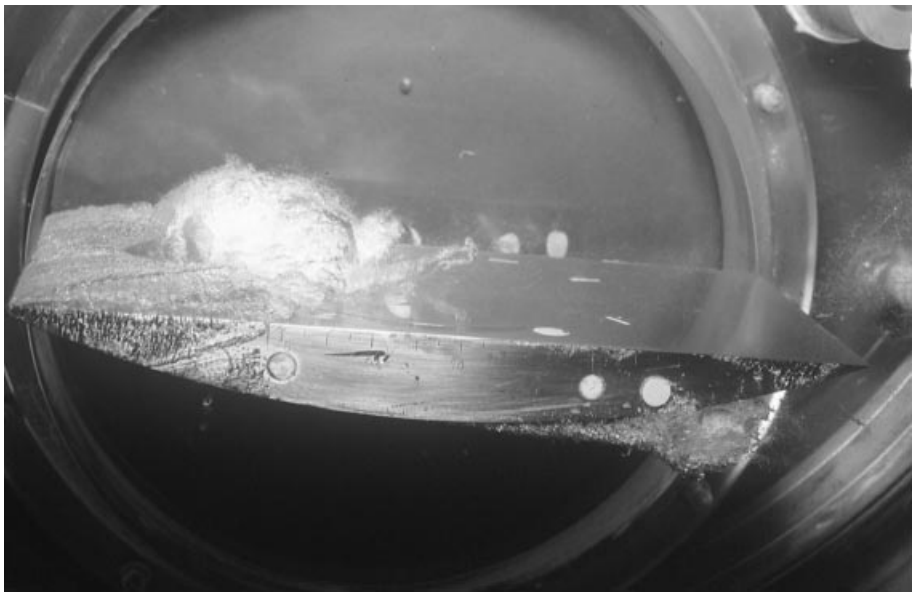

FIGURE 4. Typical view of the re-entrant jet instability and associated cloud cavitation on a plano-convex hydrofoil (angle of attack 3°, cavitation number 0.54, Reynolds number 2×10^6, maximum cavity length ≈ 72 mm, flow is from left to right).

between adjacent layers could prevent the re-entrant jet counterflow developing up to the leading edge.

The present paper is devoted to an analysis of the re-entrant jet instability. The major question which is addressed is the physical origin of this instability: what makes a re-entrant jet develop in the closure region of a partial cavity and lead it to auto-oscillate? Why are some partial cavities stable and others unstable? In connection with this key question, some of the features of this instability are analysed in more detail, such as the re-entrant jet thickness and the frequency content of the instability.

The experimental facility and the geometry tested are presented in § 2. The various cavitation patterns are given in § 3 with a special emphasis on the domain of auto-oscillations. The fundamental role of the adverse pressure gradient in the re-entrant jet instability is demonstrated in § 4 by varying the geometry and using LDV measurements. § 5 is devoted to the presentation of the re-entrant jet thickness measurements by an ultrasonic technique, and their analysis on the basis of a simple approximate model. Pressure fluctuation measurements and corresponding spectra are given and discussed in § 6.

2. Experimental conditions and general features of the flow

2.1. *Test section*

Cloud cavitation can be generated either by a hydrofoil or in a Venturi nozzle. In both cases, the same physical mechanisms are involved, as proved by the present study and the corresponding visualizations. In particular, the Strouhal numbers are similar for both geometries. Hydrofoils have the advantage of a geometry closer to the practical applications encountered in turbomachinery. However, the drawback of hydrofoil cavitation is that some critical parameters, such as the cavity thickness and

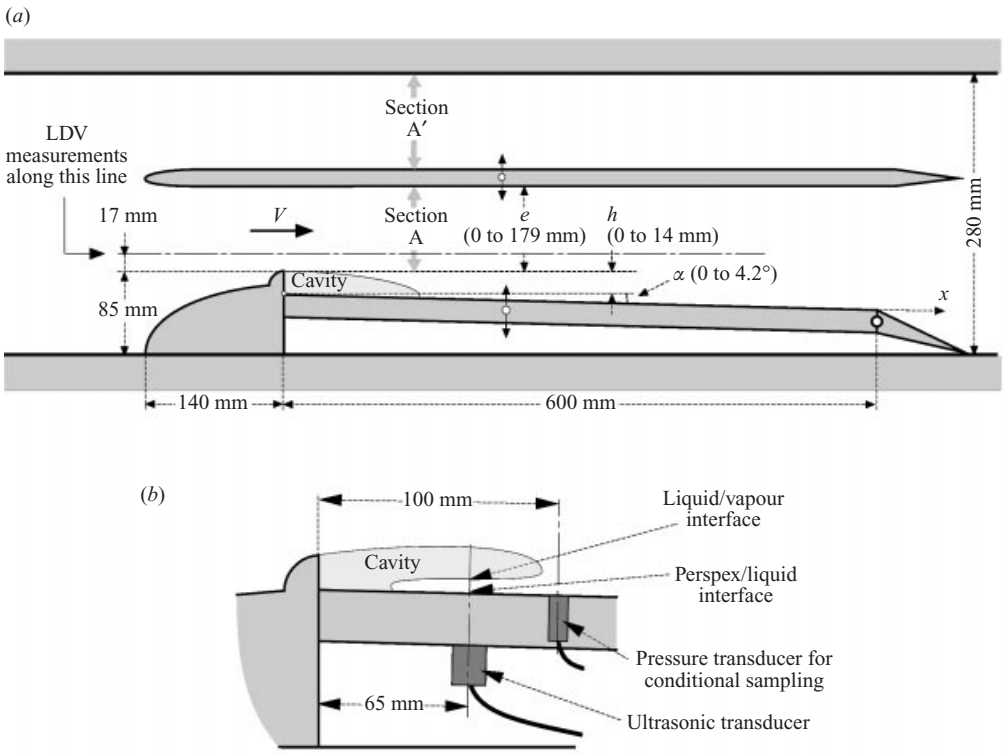

FIGURE 5. (*a*) Schematic view of the test section. The width of the channel is 175 mm. The parameters e, h and α are adjustable. The abscissa x is measured along the lower plate from the origin of the step. For the computation of the cavitation parameter, the reference pressure is measured upstream, in the middle of the test section, and the reference velocity is equal to the flow rate divided by the total area $A + A'$. The characteristic velocity V in the lower channel was measured by LDV in the middle of section A at $x = 0$. (*b*). Location of the ultrasonic transducer for the measurement of the re-entrant thickness.

the mean pressure gradient at closure, are only indirectly controlled, by way of the angle of attack.

For the study we planned, it was necessary to control both parameters as directly as possible. A special test section was built, made of a diverging step of adjustable height h. As shown on figure 5, an additional horizontal plate was set above the step to change the confinement of the flow, measured by the distance e. The slope α of the lower plate is also adjustable to change the divergence of the channel.

This final geometry resulted from several preliminary tests. Without the upper plate, no auto-oscillations at all were observed. This unexpected fact lead us to conjecture that the pressure gradient in the cavitating channel might play a prominent role in the re-entrant jet instability. The upper confinement plate was added and auto-oscillations could then be observed. Note that the quarter of circle at the back of the elliptical nose is a legacy of these preliminary tests and is of no importance.

The tests were conducted in the hydrodynamic tunnel at our institute (Briançon-Marjollet & Michel 1990). The size of the test section is $0.28\,\mathrm{m} \times 0.175\,\mathrm{m}$. Most tests were carried out at a flow velocity of $11.6\,\mathrm{m\,s^{-1}}$ measured by laser Doppler velocimetry (LDV) in the middle of the minimum section of the lower channel, at

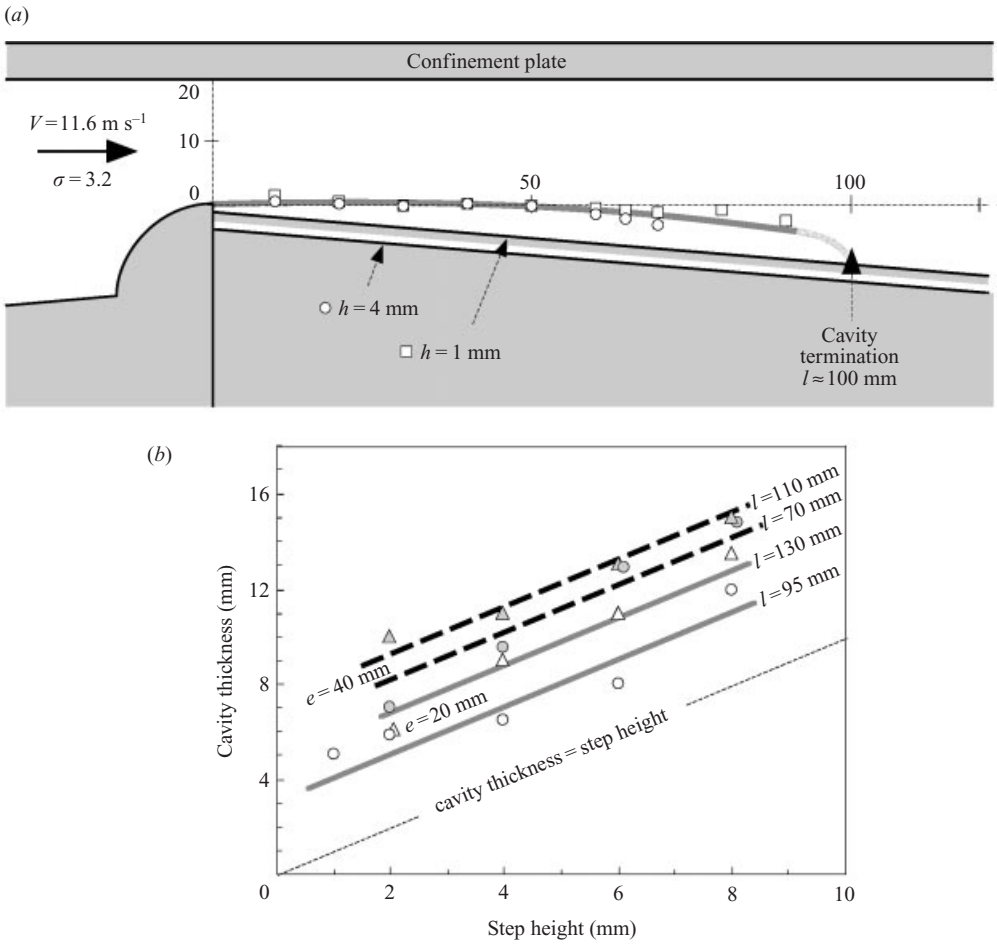

FIGURE 6. Mean cavity thickness for a flow velocity of 11.6 m s^{-1} and a divergence angle of 4.2°. (*a*) Profiles of the cavity for two different values of the step height. The case $h = 4$ mm corresponds to cloud cavitation. In this case, the cavity termination remains undefined due to the strong unsteadiness at closure. (*b*) Variation of the cavity thickness at the abscissa $x = 65$ mm (location of the ultrasonic transducer) with the step height for two different confinements and various cavity lengths.

the abscissa $x = 0$. The cavity length is controlled by the cavitation number, which is changed by changing the ambient pressure.

An important feature of the tunnel for the investigation of unsteady cavitation is the existence of two large downstream tanks with a free surface. They limit the effect of coupling between the flow in the test section and in the rest of the facility. They contribute to counterbalancing the variations in time of the cavity volume.

The use of an adjustable height h results from previous experiments on hydrofoils (Le *et al.* 1993*a*) which led us to conjecture that auto-oscillations occur only for thick enough cavities. The height h of the step is an easy way to control the cavity thickness. Figure 6(*a*) gives a comparison of the contours of two cavities of same length for two different step heights and the same confinement. These profiles were obtained by simple observation under backward continuous lighting. Figure 6(*a*) shows that the contour of the cavity is almost independent of the step height and, as a result, the

cavity thickness depends directly on the position of the lower plate. If the plate is lowered, the cavity thickens as much. Figure 6(*b*) presents the evolution, with the step height, of the cavity thickness measured at the location of the ultrasonic transducer, 65 mm downstream the cavity leading edge. These data are used later to get a non-dimensional value of the re-entrant jet thickness. Figure 6(*b*) confirms, although the error is non-negligible, that the cavity thickness varies linearly with the step height. For a given cavity length, the offset depends upon the degree of confinement. The more confined the flow, the more flattened the cavity, as we could expect. At this fixed location, figure 6(*b*) also shows that the cavity thickness tends to increase with the cavity length, which is a quite natural trend. From these prior tests, we conclude that the step height is a relevant parameter to control the cavity thickness.

2.2. *Velocity measurements and pressure gradient estimates*

In addition to the step height h, two other parameters can be changed: the confinement height e and the divergence angle α. An elementary approach based on the Bernoulli equation in a one-dimensional channel, and neglecting h, shows that the gradient of the pressure coefficient at $x = 0$ is given by

$$\frac{\mathrm{d}C_p}{\mathrm{d}x} = \frac{2\tan\alpha}{e}. \tag{1}$$

As expected, the confinement and the divergence both increase the adverse pressure gradient.

To confirm this qualitative behaviour, it was decided to conduct an experimental evaluation of the pressure gradient in the lower channel. Moreover, systematic estimates of the adverse pressure gradient were performed for all the investigated cavitating regimes in order to correlate the development of the re-entrant jet with the pressure gradient.

These estimates are based on velocity measurements. We could have used pressure taps along the upper plate to determine directly the pressure distribution in the lower channel below the confinement plate, but it was easier for us to use LDV. We chose to measure the horizontal flow velocity at different stations along the channel and to compute the pressure gradient from the following relation:

$$\frac{\mathrm{d}p}{\mathrm{d}x} = -\rho U\frac{\mathrm{d}U}{\mathrm{d}x}. \tag{2}$$

The measurements were made along a horizontal line shown in figure 5, situated 17 mm above the downstream end of the front nose. Although the choice of this measuring line is somewhat arbitrary, it fulfils two basic conditions. First, the measuring points are outside the boundary layer of the confinement plate for all cases. Secondly, in the cavitating case, the estimated pressure gradient must not be influenced by the local singularity of the cavity closure. So, the measurements must be made sufficiently far from the cavity itself. In the most confined situation investigated here, which corresponds to $e = 20$ mm, it appeared satisfactory to carry out the measurements along the confinement plate 3 mm from it, and in all other cases, the same measuring line was considered. In the cavitating case, the pressure gradient estimated on this line, at the abscissa of cavity closure, is called the 'pressure gradient at closure'. The value so defined is considered as representative of the pressure gradient in the test section at the abscissa of cavity closure.

Returning to the general features of the flow, the estimates of the pressure gradient obtained by the above procedure in the non-cavitating case confirm the increase

of the pressure gradient with an increase either in the divergence angle or in the confinement subsequent to a reduction of e. The measurements also show that the adverse pressure gradient is smaller downstream. This observation is fundamental to understand the dynamic behaviour of the longer cavities, as discussed in § 6.

In addition to mean values, the fluctuations of the velocity were measured by LDV. In the cavitating regimes, the most important source of fluctuations is the cavity itself. The 'velocity fluctuations at closure' used below are defined as the ratio of the RMS velocity fluctuations measured on the same line at the abscissa of cavity closure to the mean velocity at the same point. The objective of these measurements was to characterize the degree of unsteadiness of the cavity, which is expected to be particularly important for cloud cavitation (cf. § 3).

In order to characterize the frequency content of the cavity oscillations, pressure fluctuations were measured. Five PCB piezoelectric transducers (model H111A21) with a sensitive surface of 5.5 mm in diameter and a rise time lower than 2 μs were mounted flush with the lower plate, at the locations $x = 50$, 75, 100, 125 and 150 mm measured from the origin of the step.

2.3. *Re-entrant jet thickness measurements*

The dynamic behaviour of a partial cavity differs according to the relative orders of magnitude of the thicknesses of the re-entrant jet and of the cavity. Therefore, it is necessary to be able to measure the re-entrant jet thickness.

In the present experiments, an ultrasonic technique was developed to measure the thickness of the liquid layer which lies just below the cavity. An ultrasonic transducer (PANAMETRICS ref. V306-SU and V311-SU) was set on the lower plate together with a pressure transducer, which is necessary for conditional sampling (cf. figure 5*b*). The transducer emits a limited waveform signal at a frequency of 2.25 MHz or 10 MHz, according to the model used, and detects the different echoes coming back from the various interfaces. From the measurement of the time difference Δt between the two echoes coming from the interfaces Perspex/liquid and liquid/vapour, we can determine the liquid layer thickness δ by the simple relation

$$\delta = \frac{c_s \Delta t}{2}, \tag{3}$$

where c_s is the sonic velocity in the liquid.

As the existence of the re-entrant jet is not permanent but periodic, the measurements are conducted at various instants in the auto-oscillation cycle by means of the pressure transducer, which gives a reference pulse, connected to a system of variable time delay. Therefore, the evolution of the re-entrant jet thickness throughout the period can be determined. The image of the cavity is simultaneously acquired to correlate the measurements with the cavity evolution.

The system was first checked in the hydrodynamic tunnel using a layer of water of known thickness at rest on the lower plate. In particular, the influence of the incidence angle of the ultrasonic beam and of the shape of the interface on the response of the transducer was qualitatively analysed. It was observed that the amplitude of the echo is reduced by an inclination of the incident beam and also by perturbations travelling on the interface. Both effects were not further investigated as they did not appear critical for the intended measurements.

The determination of the liquid layer thickness relies on the sonic velocity. We can expect a difficulty in cavitating flows as it is well-known that the sonic velocity depends upon the void fraction. Although the re-entrant jet is expected to be mainly

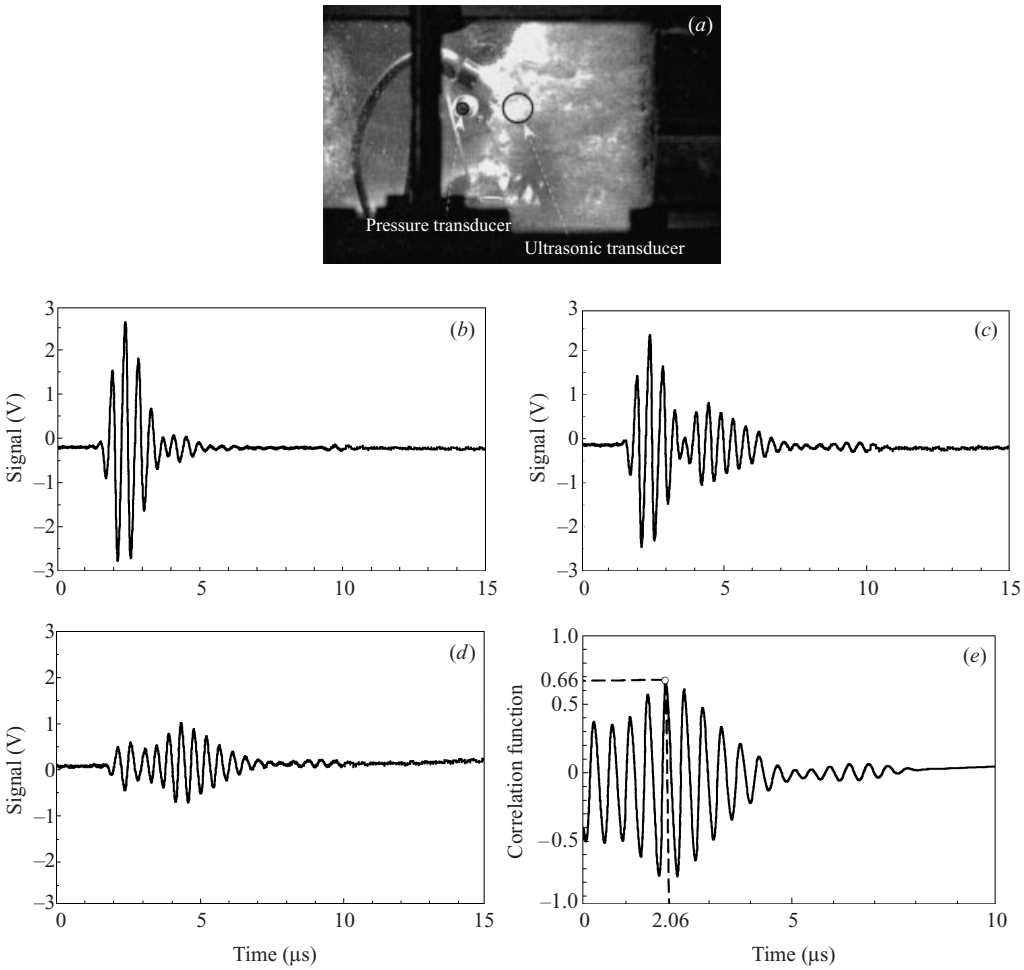

FIGURE 7. Principle of the measurement of the re-entrant jet thickness with an ultrasonic transducer. Step height $h = 4$ mm, confinement $e = 20$ mm, divergence angle 4.2°, flow velocity 11.6 m s^{-1}, ultrasonic transducer frequency 2.25 MHz. (*a*) View of the cavity at the instant of the measurement (flow from right to left). (*b*) Reference signal of the ultrasonic transducer under non-cavitating conditions. (*c*) Signal at the cavitating conditions corresponding to (*a*). (*d*) Difference between the cavitating and non-cavitating signals (*b*) and (*c*). (*e*) Correlation of the signal difference (*d*) with the the non-cavitating signal (*b*).

of liquid nature, it may contain cavitation bubbles which may change the sonic velocity. The effect of the void fraction on the sonic velocity is usually approached on the basis of homogeneous models, with or without phase change (see e.g. Brennen 1995). Such models, which predict a drop of the sonic velocity with the void fraction, are valid only if the size of the inhomogeneities is much smaller than the wavelength. This condition is necessary to justify the assumption of a homogeneous representation of the two-phase mixture. In the present case, the ultrasonic frequencies are 2.25 MHz or 10 MHz and the wavelengths are respectively 0.66 mm and 0.15 mm. From our knowledge of such cavitating flows, we can expect bubbles of the same order of magnitude as the wavelength, so that the homogeneous model is not relevant of the present situation. To have an idea of the influence of relatively large bubbles on the sonic velocity, a few tests were done using a liquid layer of known thickness in

which electrolysis bubbles were produced. No deviation from the sonic velocity for the pure liquid was observed. Hence it was concluded that, even if there were cavitating bubbles in the re-entrant jet flow, they would not have any influence on the acoustics of the liquid in the present domain of wavelengths.

In practice, the time interval Δt is determined from the correlation between a reference ultrasonic signal under non-cavitating conditions, and the difference between the cavitating and non-cavitating signals (see figure 7). From the correlation, two parameters are obtained: the maximum value of the correlation coefficient and the corresponding time interval Δt used in (3) for the determination of the liquid layer thickness.

For given conditions, about 50 similar measurements were done and the mean and RMS values were calculated. In addition, a validation rate was defined as the percentage of measurements leading to a correlation coefficient greater than 0.5. The measurements associated with a smaller value of the correlation coefficient were considered as of poor quality and were rejected.

Most results presented in this paper were obtained with the 2.25 MHz ultrasonic transducer. Due to the relatively small thickness of the re-entrant jet (of the order of 1 mm), the two echoes are only 1 to 2 μs apart and may partially overlap. In order to better separate the echoes, we also used a 10 MHz transducer which emits a shorter burst. Although the measuring conditions seem more satisfactory at a higher frequency, the measurements proved to be more difficult in practice due to a smaller amplitude of the signal. Actually, the 10 MHz transducer was not used extensively: it just allowed us to confirm the measurements given by the 2.25 MHz transducer. The agreement on the re-entrant jet thickness is better than 5%.

3. Cloud cavitation and surrounding regimes

Different regimes of partial cavitation were observed on the present backward diverging step according to the values of the cavitation number and of the three adjustable geometric parameters of the test section. As a reference, we consider the case of a confinement height $e = 20$ mm and a diverging angle $\alpha = 4.2°$. The influence of both parameters will be examined in § 4. The mapping of the regimes is given in figure 8 as a function of the cavitation number and of the height of the step h.

The central part of the diagram corresponds to auto-oscillating cavities. As proved by the visualizations presented in figure 9 and discussed later, this domain is the one of the re-entrant jet instability and subsequent cloud cavitation. It can easily be identified visually as the shedding is periodic and can be frozen under stroboscopic lighting. At its limits, the shedding loses its regularity. We generally observe an intermittency between coherent bursts of large clouds and a chaotic entrainment of smaller vapour structures. This latter regime finally prevails outside the domain of cloud cavitation.

In its upper part, i.e. for large step heights and for large cavitation numbers (domain 5), the region of cloud cavitation is limited by shear cavitation. As expected, the vapour does not fill all the space behind the step but is limited to the shear layer. At the limit between cloud cavitation and shear cavitation, the ratio between the cavity length and the step height lies between 6 and 10. This value is comparable to the normalized mean reattachment length behind a rearward facing step in non-cavitating flows, which is of the order of 7 (Driver & Seegmiller 1985; Eaton & Johnston 1981; Jovic & Driver 1995; Kim, Kline & Johnston 1980). At the upper right limit of the domain of cloud cavitation, the structure of the cavitating flow

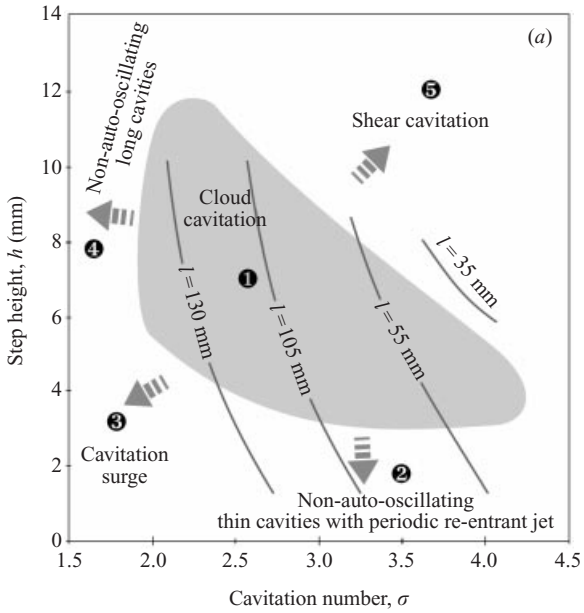

FIGURE 8. Mapping of the cloud cavitation instability and surrounding cavitation regimes for a flow velocity of $11.6\,\mathrm{m\,s^{-1}}$, a confinement height $e = 20\,\mathrm{mm}$ and a divergence angle of 4.2°. (*a*) obtained from direct observation of cavitation patterns under stroboscopic lighting; (*b*) obtained from velocity fluctuation measurements.

is chiefly imposed by the subcavitating flow. On the other hand, the cavity length normalized by the step height is much higher in the cloud cavitation regime. It exceeds 30 at low step heights and low cavitation numbers. In such a case, the development of cavitation totally transforms the basic subcavitating flow.

On the left-hand side of figure 8, i.e. for small cavitation numbers (domains 3 and 4), the cavities are long. They close in a region of small adverse pressure gradient as mentioned in § 2. No re-entrant jet is observed, and the entrainment of vapour in the wake is much more continuous than in the case of periodic cloud shedding. At the bottom (domain 3), the cavities are the longest. They close in a region of nearly constant pressure, so that they can extend very easily in the lower channel without experiencing any substantial resistance. This is the case of an extreme sensitivity to fluctuations discussed in the introduction, which can lead to oscillations of the cavity. It is important to be aware that such oscillations are not triggered by a re-entrant jet, which actually does not exist. This behaviour is of surge type and depends upon the research facility. Its frequency content will be discussed in § 6.

In its lower part, the domain of auto-oscillations is limited by a regime (domain 2) in which the cavity length is no longer oscillating but a re-entrant jet still exists as can be seen on the visualizations presented in figure 10. Such a behaviour is unexpected as the existence of the re-entrant jet is generally associated with cavity oscillations and cloud cavitation. Although the cavity has no periodic behaviour and has an approximately fixed length, visualizations by ultra-rapid films have proved that the behaviour of the re-entrant jet is actually periodic. The period is close to the one measured in the case of cloud cavitation.

Because of the somewhat subjective way of determining the extent of the regime of cloud cavitation from visual observations, another technique was used. The velocity

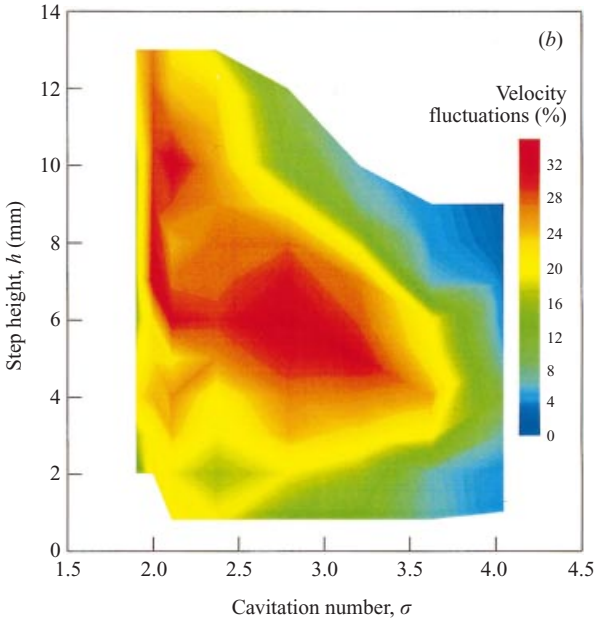

FIGURE 8(*b*). For caption see facing page.

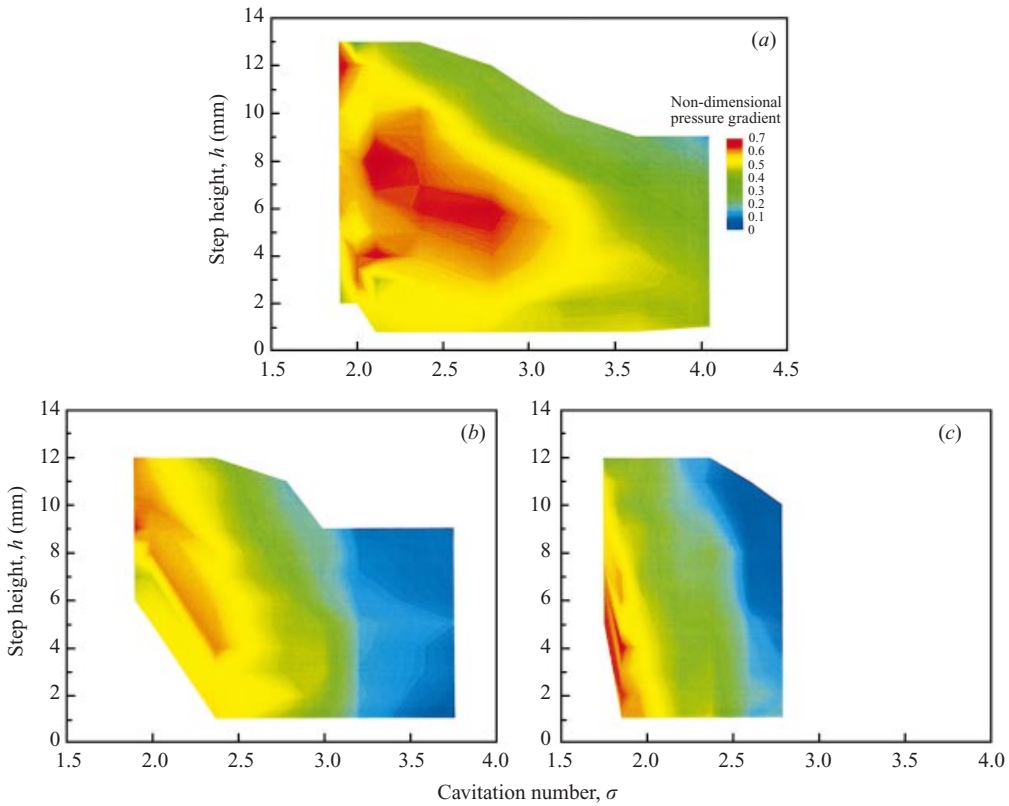

FIGURE 14. Estimates of the pressure gradient at closure. Influence of the confinement height at divergence angle 4.2°. The pressure gradient is non-dimensionalized by the cavity length. (*a*) Flow velocity 11.6 m s^{-1}, confinement height 20 mm, (*b*) flow velocity 9.6 m s^{-1}, confinement height 40 mm; (*c*) flow velocity 8.5 m s^{-1}, confinement height 60 mm.

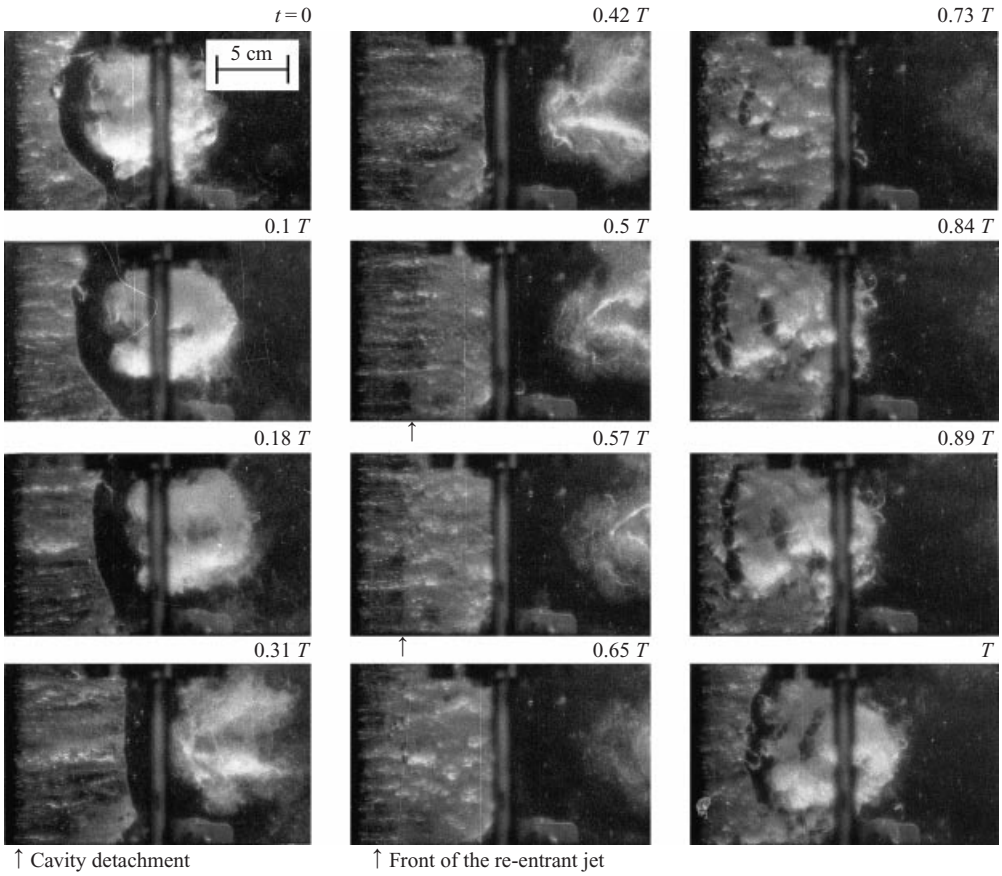

FIGURE 9. Visualization of the re-entrant jet and of the cavity auto-oscillations (cloud cavitation). Flow velocity 11.6 m s^{-1}, confinement height $e = 20$ mm, step height $h = 3.6$ mm, divergence angle 4.2°. The period of the oscillation is 35 ms. The flow is from left to right.

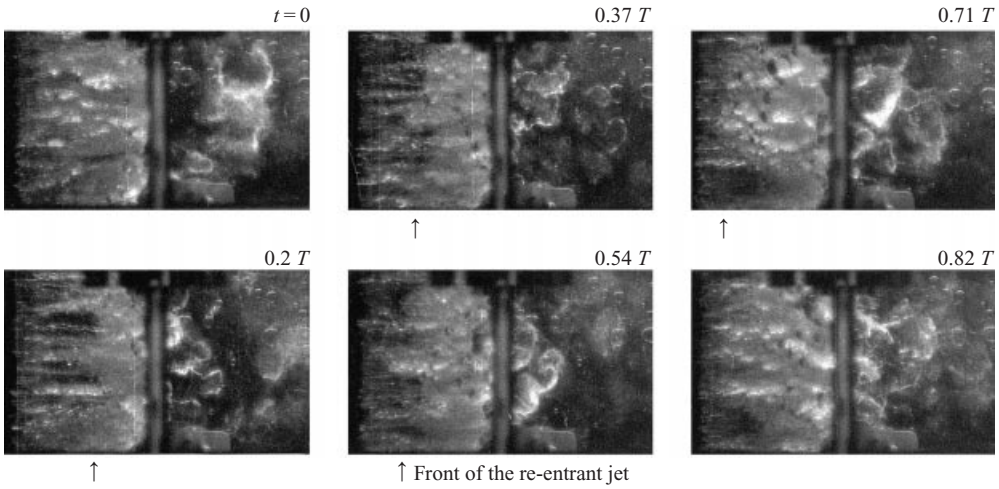

FIGURE 10. Visualization of the case of thin cavities (domain 2). Flow velocity 11.6 m s^{-1}, confinement height $e = 20$ mm, step height $h = 0.8$ mm, divergence angle 4.2°. The period of the oscillation is 36 ms. The flow is from left to right.

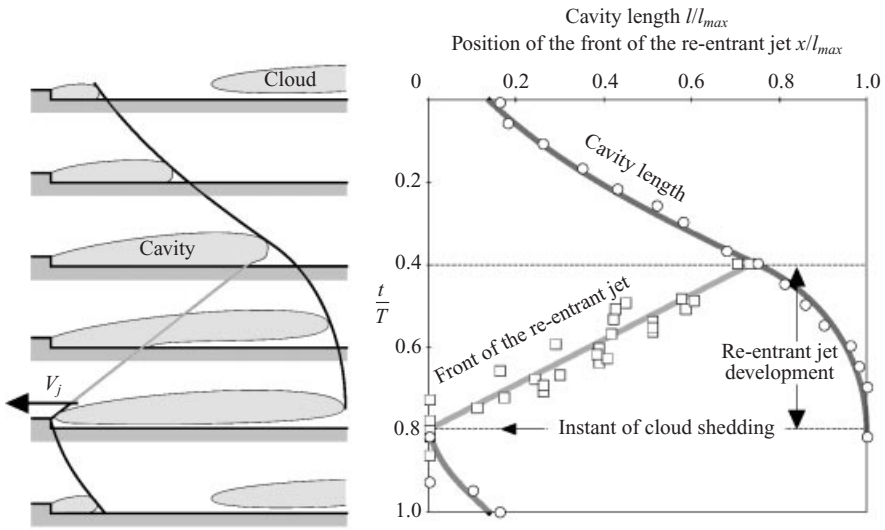

FIGURE 11. Evolution of the cavity and the re-entrant jet in the case of the cloud cavitation instability (domain 1 of figure 8). Flow velocity 11.6 m s^{-1}, confinement height $e = 20$ mm, divergence angle $\alpha = 4.2°$, step height $h = 3.6$ mm, cavitation number $\sigma = 3.2$, maximum cavity length $l_{max} = 100$ mm, period of oscillation $T = 35$ ms, Strouhal number $S = 0.25$.

fluctuations at closure were systematically measured and isovalues were plotted on the same diagram (figure 8*b*). On comparing figures 8(*a*) and 8(*b*), it appears that the domain of high-velocity fluctuations corresponds pretty well to the domain of cloud cavitation identified visually. Velocity fluctuations at closure exceed 30% at the centre of the domain of cloud cavitation. Outside, they are of the order of 10%. A threshold of about 22% gives a good match to the visual limits of the regime of cloud cavitation. Slight differences are visible. In particular, velocity fluctuations remain intense in domain 3 of surge cavitation where the cavity undergoes oscillations due to another kind of instability. The agreement between these two ways of determining the domain of cloud cavitation was confirmed for several other operating conditions. It gives some confidence in the visual determination of the domain of the re-entrant jet instability.

In the regime of cloud cavitation, the dynamic behaviour of the cavity is classical (see figure 9). On the images corresponding to $0.84T$ to T and 0 to $0.42T$ (where T is the shedding period), the attached cavity grows with a well-defined closure line. On images $0.5T$ to $0.65T$, the front of the re-entrant jet (indicated by an arrow) is visible. It moves upstream and reaches the cavity leading edge approximately on the image corresponding to time $0.73T$. At this time, the length of the cavity is maximum. Then, the re-entrant jet cuts off the interface and the major part of the attached cavity becomes a cloud which detaches from the foil. At the instant of shedding, the length of the attached cavity is almost zero. Then it grows again and a new cloud is shed.

The evolution with time of the cavity length and of the front of the re-entrant jet are shown on figure 11. The growth rate of the cavity length is almost linear until the re-entrant jet initiates, and afterwards, it declines. The velocity of the re-entrant jet can be considered as nearly constant all along its development. It covers a distance of about 75% of the maximum cavity length l_{max} during a time of about 40% of the shedding period T. Hence, its mean velocity V_j is of the order of $0.75l_{max}/0.40T \approx 1.9l_{max}/T$. Using the definition of the Strouhal number based on the maximum cavity length,

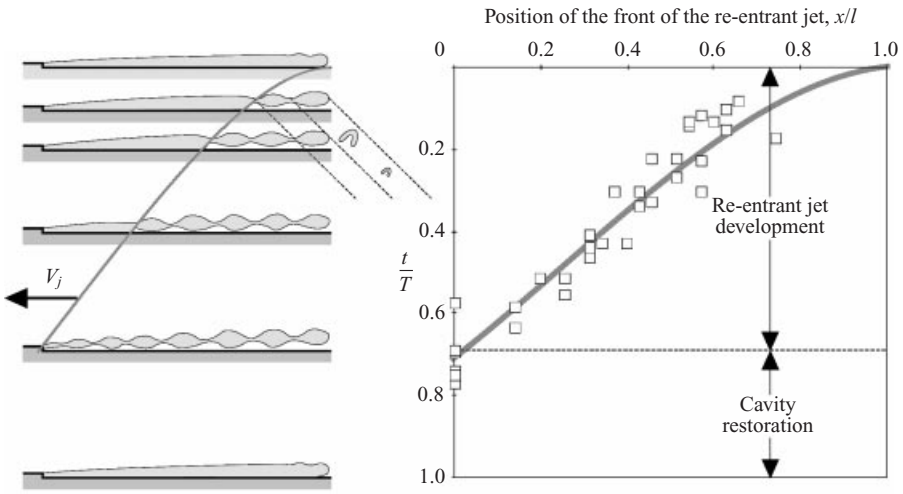

FIGURE 12. Evolution of the cavity and the re-entrant jet in the case of a thin cavity with a re-entrant jet (domain 2 of figure 8). Flow velocity 11.6 m s^{-1}, confinement height $e = 20$ mm, divergence angle $\alpha = 4.2°$, step height $h = 0.8$ mm, cavitation number $\sigma = 3.2$, Cavity length $l = 100$ mm, period of the re-entrant jet $T = 38$ ms.

$S = fl_{max}/V$, we can relate the Strouhal number to the ratio of the re-entrant jet velocity to the upstream velocity by the equation $S \approx V_j/1.9V$. As the Strouhal number of this instability is classically about 0.25, we obtain that the velocity of the re-entrant jet is about half the mean flow velocity. This value corresponds to the measurements of Pham *et al.* (1998) on a hydrofoil, using electrical probes. It confirms that the mechanism of cloud cavitation on a backward facing step is similar to that on a hydrofoil.

The regime observed in region 2 relates to small step heights, i.e. to thin cavities. This is the main reason for the difference with the auto-oscillating case. In the latter case, i.e. for thick enough cavities, the re-entrant jet, which is thin in comparison with the cavity, does not interact significantly with the cavity interface as it moves upstream. The interaction is limited to the instant at which it reaches the cavity leading edge and cuts the cavity interface, i.e. at the very end of its upstream movement. When the cavity thickness approaches the re-entrant jet thickness, i.e. as the step height is reduced, a significant interaction exists between the cavity interface and the re-entrant jet, all along its upstream movement. This is the case in domain 2. This interaction is firstly characterized by a smaller velocity of the re-entrant jet, as if it were slowed by the cavity interface. It can be seen on figure 12 that the velocity of the re-entrant jet can still be considered as approximately constant, except at the very beginning. It takes about 70% of the period for the re-entrant jet to cover about 80% of the cavity length. Therefore, its velocity is about $1.1l/T$, which gives a ratio V_j/V of about 0.3, to be compared to 0.5 in the auto-oscillating case. In this regime of thin cavities, the re-entrant jet velocity is only 60% of its velocity in the regime of cloud cavitation.

Secondly, because of the closeness of the cavity interface and the upper boundary of the re-entrant jet, the small-scale instabilities which develop on both interfaces make the thin vapour layer break at many points. Many small vapour structures are formed, as schematically shown on figure 12, and entrained by the liquid flow. The cavity is made of a two-phase mixture very different from its almost pure vapour content during the phase of cavity growth in the auto-oscillating case.

We noticed that the re-entrant jet velocity is lower in the case of thin cavities than in the case of auto-oscillations, whereas the global periods are almost the same. Hence, the cavity requires less time to restore. Actually, the restoration mechanism is different. We have seen that, in the case of auto-oscillations, the cavity grows from the very limited residue attached to the foil leading edge, just after cloud shedding. On the other hand, in the case of thin cavities, all the small vapour structures which develop throughout the interface during the progression of the re-entrant jet form as many residues for the restoration of the cavity. Hence it is not surprising that the restoration phase is shorter. In conclusion, this peculiar regime demonstrates the strong effect, on the dynamic behaviour of the cavity, of its thickness compared to that of the re-entrant jet.

Finally, let us note that, in the framework of the classical steady potential theory, and if we assume that the cavity interface is a constant-pressure line, the flow velocity over the cavity, which is also the re-entrant jet velocity, should be equal to $\sqrt{1+\sigma}V_\infty$. Therefore, the re-entrant jet velocity should be larger than the flow velocity at infinity V_∞. The present experimental results are inconsistent with this conclusion and show the limitations of steady potential theory. The unsteadiness of the flow as well as friction on the wall or between interfaces could contribute to explaining a smaller re-entrant jet velocity.

4. Re-entrant jet instability and adverse pressure gradient

Once the domain of development of the re-entrant jet instability is clearly identified as a function of the operating conditions, the next question is to find the critical parameters which control this instability. In a first step, this was done by changing the tested configuration, which is possible by varying either the degree of confinement by the upper plate or the divergence angle of the lower one.

Figure 13 shows how these two parameters influence the domain of auto-oscillation. It appears that its extent is considerably reduced if the confinement height is increased or if the divergence angle is decreased. For a confinement height above about 60 mm and in particular in the non-confined case, no cloud cavitation at all was identified visually.

It was seen in § 2 that a reduction in the confinement height and an increase in the divergence angle both result in an augmentation of the adverse pressure gradient in the test section. Therefore, it is clear that a correlation exists between the re-entrant jet instability and the adverse pressure gradient in the channel.

To strengthen this conclusion, the mean value of the pressure gradient was systematically estimated at cavity closure, using the procedure given in § 2, and the region of high pressure gradient was compared to the domain of auto-oscillations. The best correlation is obtained if the gradient of the pressure coefficient is non-dimensionalized by the cavity length, thus introducing the variable $\mathrm{d}C_p/\mathrm{d}(x/l)$. This parameter also appears quite naturally in the physical modelling presented in the Appendix.

Results are given in figure 14 (see p. 237) for three different geometries of confinement. In each case, the pressure gradient at closure is large inside the region of auto-oscillations. Although the domain of high pressure gradient at closure does not superpose exactly on that of auto-oscillations, there are strong similarities between the two. It is clear that the region of high pressure gradient considerably shrinks when the confinement height e increases, as is the case for cloud cavitation. In particular, in the less confined situation ($e = 60$ mm, figure 14*c*) for which no cloud cavitation could be discerned visually, the region of high pressure gradient at

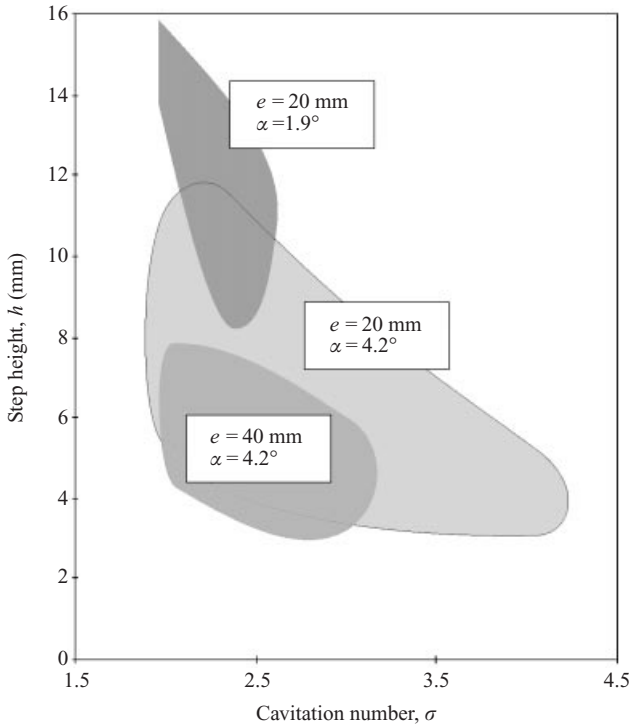

FIGURE 13. Evolution of the extent of cloud cavitation for different operating conditions at a flow velocity of 11.6 m s^{-1}.

closure is extremely reduced in comparison with the more confined case ($e = 20$ mm, figure 14*a*).

These observations confirm, at least qualitatively, the critical role of the adverse pressure gradient in the onset of the re-entrant jet instability. From a physical viewpoint, it is concluded that an adverse pressure gradient is favourable to the development of the re-entrant jet. A simple model developed in the Appendix supports this interpretation. This model provides an analysis of the influence of the adverse pressure gradient on the thickness of the re-entrant jet. It is a simplified one which is partly based on a dimensional analysis and which does not take into account unsteady effects. It allowed us to obtain easily some key results without developing a complex model of the full cavitating flow. The conclusions are summarized by equation (A 8):

$$\delta \approx \delta^* + \frac{1}{4}\frac{\mathrm{d}C_p}{\mathrm{d}(x/l)}\, d. \tag{4}$$

This equation gives an estimate of the re-entrant jet thickness δ in the presence of a pressure gradient $\mathrm{d}C_p/\mathrm{d}(x/l)$. The quantity δ^* is the thickness of the re-entrant jet without any pressure gradient and d is the cavity thickness.

From (4) it is clear that the thickness of the re-entrant jet is increased by an adverse pressure gradient. On the other hand, a negative pressure gradient will reduce it and may even make it vanish if it is large enough. So, this simplified analysis, which is valid only for a steady situation, confirms the predominant role of the pressure gradient in the re-entrant jet and consequently in the cloud cavitation instability. Recall that it is not the only parameter to influence this type of instability and that

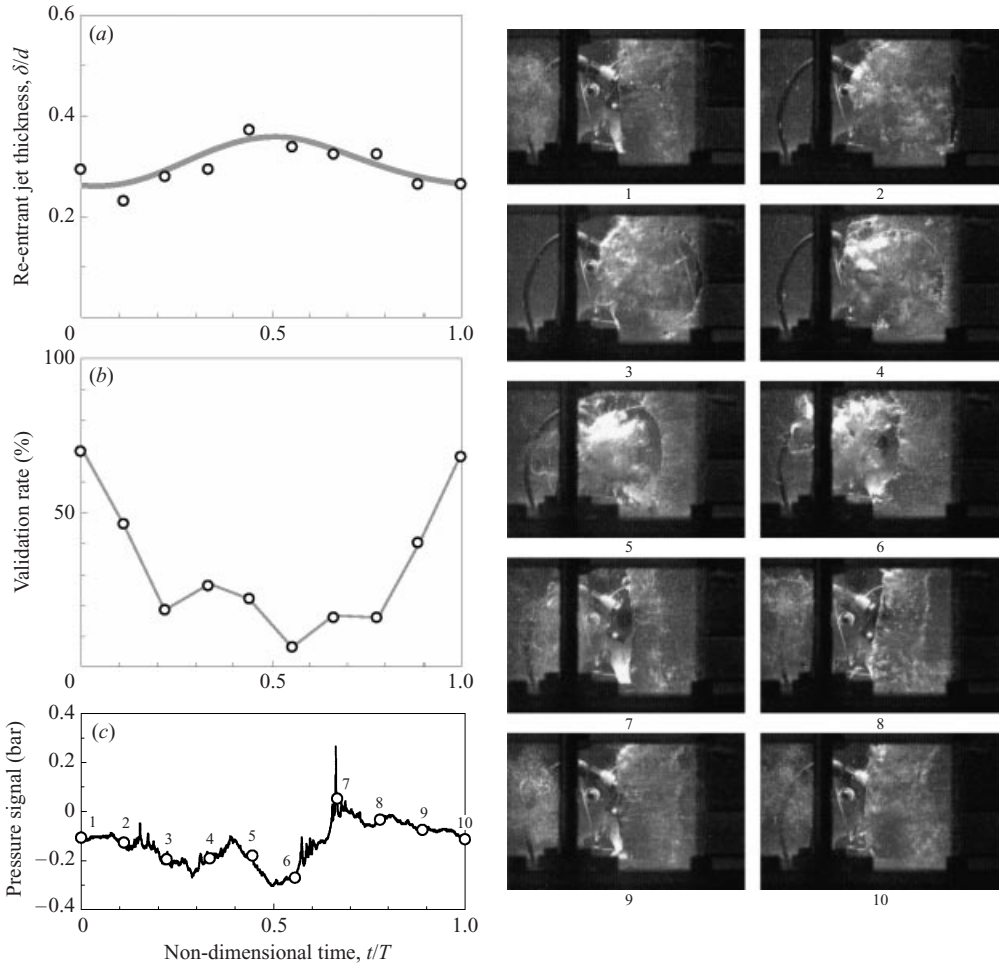

FIGURE 15. Evolution of the liquid film thickness during a typical period of oscillation. Flow velocity 11.6 m s^{-1}, confinement height $e = 20$ mm, divergence angle $\alpha = 4.2°$, step height $h = 4$ mm, cavitation number $\sigma = 3.2$, maximum cavity length $l_{max} = 100$ mm, period of oscillation $T = 36$ ms, flow from right to left. (*a*) Re-entrant jet thickness; (*b*) validation rate; (*c*) pressure signal. Photographs 1 to 10: views of the cavity at 10 instants during the period shown on (*c*).

an additional condition on the thickness of the re-entrant jet compared to that of the cavity is required for this instability to actually occur (see § 3). The next section is devoted to the measurement of the re-entrant jet thickness and the comparison with the estimates obtained from (4).

5. Re-entrant jet thickness

The ultrasonic technique developed in this work was systematically used to measure the thickness of the re-entrant jet under various conditions. It was complemented by visualizations which allow one to distinguish between a re-entrant jet and a simple liquid layer lying between the wall and the vapour region.

Results which are typical of the auto-oscillation domain are given in figure 15. The validation rate oscillates between about 70% and a few percent only, during the

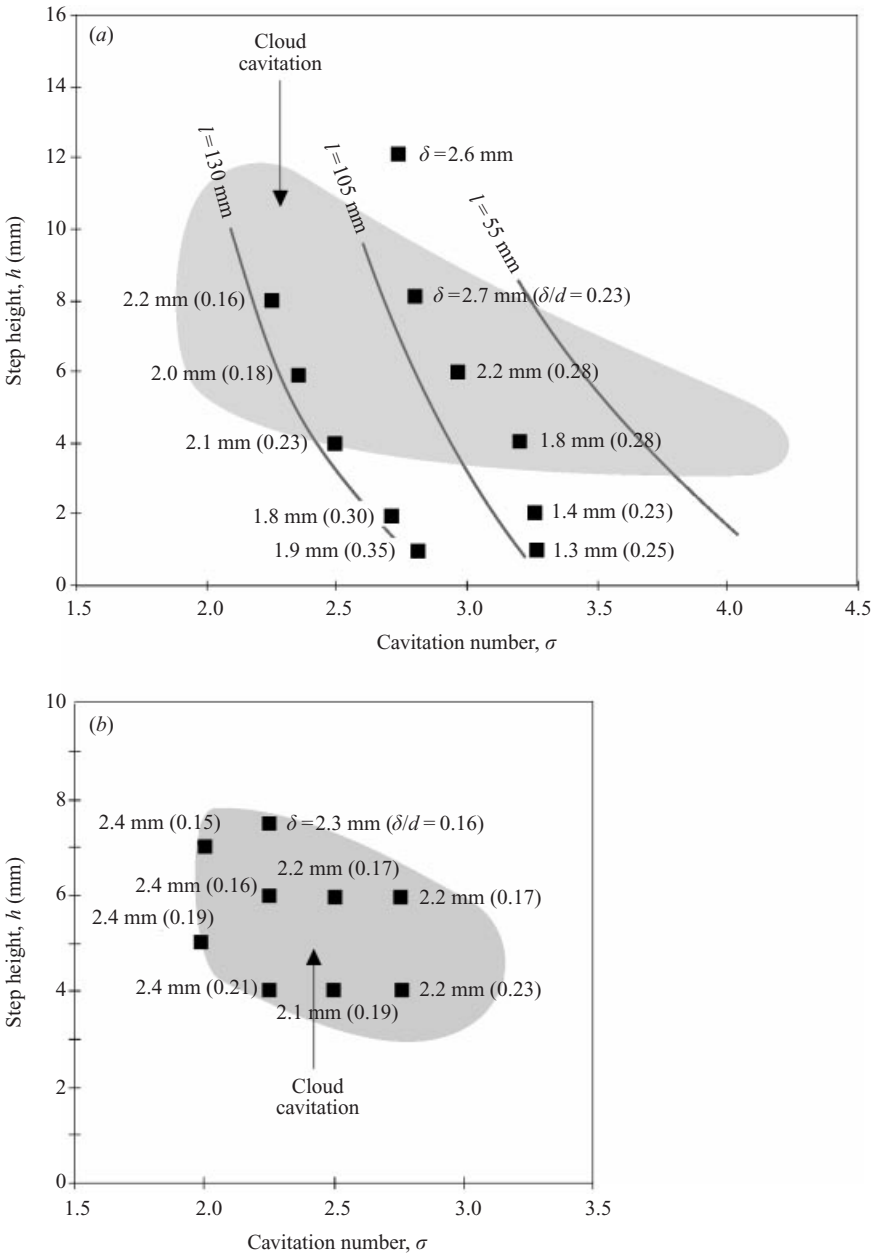

FIGURE 16. Results of the measurement of the re-entrant jet thickness. The first number gives the measured value in millimetres of the re-entrant jet thickness δ, and the number in parentheses gives the ratio of the re-entrant jet thickness δ to the cavity thickness d. The square symbols indicate the measuring points in the diagrams. For both diagrams, the flow velocity is $11.6\,\mathrm{m\,s^{-1}}$ and the divergence angle is 4.2°. (*a*) Confinement height $e = 20\,\mathrm{mm}$; (*b*) confinement height $e = 40\,\mathrm{mm}$.

oscillation cycle. If we refer to the corresponding visualizations, it appears that high validation rates are associated with instants at which a re-entrant jet actually exists on the ultrasonic transducer, whereas small validation rates occur when the cavity closes upstream of the transducer and a cavitation cloud travels over it. Although no re-

entrant jet is expected in the latter case, some rare measurements are validated. They prove that a liquid film is sometimes present below the cavitation cloud. Its thickness is only slightly greater than that of the re-entrant jet, which tends to prove that the cavity and the underlying liquid film are convected without significant morphological changes, at least at the very beginning of the shedding process. As the liquid film thickness does not change much during the whole oscillation cycle, it was decided to consider only a mean value for the discussion below.

The various measurements of the re-entrant jet thickness which were done, in the region of cloud cavitation and also for thin non-pulsating cavities with a re-entrant jet, are presented in figure 16. For a confinement height of 40 mm (figure 16*b*), the cloud cavitation domain is relatively small and the re-entrant jet thickness does not vary much over this domain; the measurements lie between 2.1 mm and 2.4 mm. In the case of a confinement height of 20 mm (figure 16*a*), the cloud cavitation domain is larger and the mean value of the re-entrant jet thickness can vary a little bit more, between 1.8 mm and 2.7 mm. In the case of thin non-pulsating cavities obtained for small step heights, the re-entrant jet is somewhat thinner, between 1.3 mm and 1.9 mm. From these measurements, it is hard to point out the detailed variations of the re-entrant jet thickness with the various operating parameters. In particular, we must keep in mind that the measurements are conducted at a fixed point corresponding to the location of the ultrasonic transducer, whereas the cavity length is obviously not constant over the whole domain of cloud cavitation. Anyhow, the present results show that, for a constant cavity length, the thickness of the re-entrant jet tends to increase with the thickness of the cavity. Like the ratio of the re-entrant jet thickness to the cavity thickness, it ranges between 15% and 35%. The largest values more often correspond to thinner cavities.

The variations of the thicknesses of the re-entrant jet and of the cavity with the step height are given in figure 17. The re-entrant jet thickness decreases slightly when the step height decreases, whereas the cavity thickness decreases much more significantly, like the step height. Hence, the vapour layer between the re-entrant jet and the external liquid flow becomes thinner and thinner as the step height decreases. It ranges roughly from 9 mm for $h = 8$ mm to 3 mm for $h = 1$ mm. We must recall that the cavitation pattern is different according to the step height. For large step heights, i.e. thick cavities, cloud cavitation is observed, whereas for small step heights ($h < 3$ mm), the partial cavity does not oscillate although a re-entrant jet still exists. This latter configuration was associated in § 3 with a stronger interaction between the two interfaces. This conclusion is consistent with the present observation of a reduction in thickness of the vapour layer which actually makes the interaction between the two free surfaces more and more likely as the step height is reduced.

The visualizations have shown that the vapour layer vanishes at several points along the cavity. To confirm this trend, it is necessary to quantify not only the mean value of the thickness of the vapour layer but also the height of the surface perturbations which travel on both interfaces. Concerning the re-entrant jet, we can get an estimate from considering the scattering of the measurements. From the extrema in the measured values of the re-entrant jet thickness, it appeared that the amplitudes of the fluctuations are asymmetric. They are smaller on the wall side than on the external one and were estimated respectively of the order of -1 mm and $+2$ mm.

To estimate the height of the surface perturbations which develop on the cavity, a laser sheet technique was used. Typical views of the cavity interface are shown on figure 18. They were obtained from a single shot of 20 ns in duration generated by

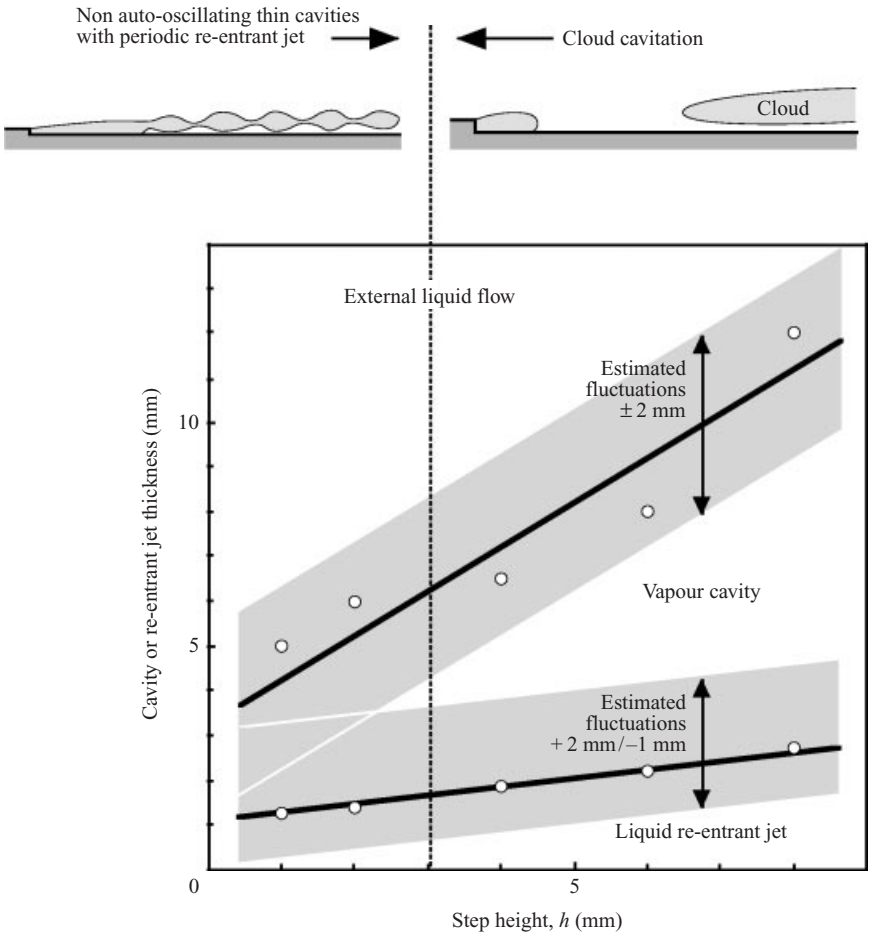

FIGURE 17. Evolution of the thicknesses of the re-entrant jet and of the cavity as a function of the step height. Flow velocity 11.6 m s^{-1}, confinement height $e = 20$ mm, divergence angle $\alpha = 4.2°$, maximum cavity length $l = 95$ mm.

a copper pulsed laser of 15 W in power. Although the size of the perturbations is variable in space and time, on average the thickness of the interface at the location of the re-entrant jet measurement was estimated to be of the order of 4 mm.

Previous estimates of the characteristic height of the perturbations which develop on both interfaces, the cavity interface and the re-entrant jet boundary, show that the interaction between the two free surfaces remains negligible provided the thickness of the vapour layer is greater than a critical value of the order of 4 mm. Taking into account the thickness of about 1 mm of the re-entrant jet, this critical vapour layer thickness corresponds to a critical cavity thickness of about 5 mm, and, in the present experimental arrangement, to a critical step height of roughly 3 mm (figure 17). The present argument clearly accounts for the lower limit of the cloud cavitation instability domain presented on figure 8.

As a result, it can be noted that cloud cavitation, which is a large-scale instability, probably depends upon smaller-scale instabilities, which in turn probably depend upon parameters such as the turbulence intensity or the surface tension. Similarly, it is likely that the interaction of the re-entrant jet with the solid wall along which

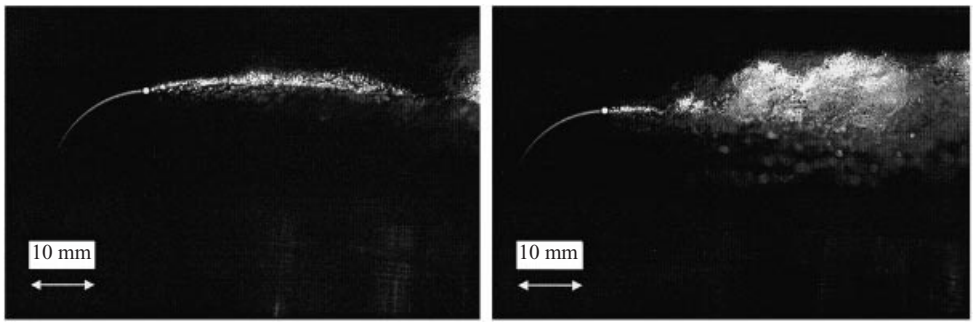

FIGURE 18. Instantaneous visualizations of the cavity interface by a laser sheet. Case of an auto-oscillating cavity at two different instants in the cycle (cloud cavitation). Flow velocity 11.6 m s^{-1}, confinement height $e = 20$ mm, divergence angle $\alpha = 4.2°$, cavitation number $\sigma = 3.2$, step height $h = 4$ mm. The flow is from left to right. The duration of the light sheet is 20 ns.

it flows may also play an important role. In the present investigation, the wall is smooth, but it was clearly proved by Kawanami *et al.* (1997) that the presence of a small obstacle can stop the re-entrant jet. Therefore, we can imagine that smaller wall surface perturbations, such as distributed roughness for instance, could significantly alter the cloud cavitation instability.

Returning to mean values of the re-entrant jet thickness, it is interesting to compare the present measurements with the estimates which can be made from the model presented in the Appendix. First, we have to estimate the thickness of the re-entrant jet without any pressure gradient by means of (A 10). The partial cavities considered here have a typical length of the order of 100 mm and a maximum thickness of the order of 10 mm, so that their non-dimensionalized length is of the order of 10. Hence, using figure 22, and considering cavities of similar shapes, we see that the non-dimensionalized thickness of the re-entrant jet, $\lambda = \delta^*/d$, is of the order of about 3%. This estimate corresponds to those computed by Laberteaux & Ceccio (1998). In any case, it is only a few percent and much smaller than the measured values which can reach 30%.

Secondly, the increase of the re-entrant jet thickness due to the adverse pressure gradient is estimated from (A 8). It is connected to the non-dimensionalized gradient of the pressure coefficient $\mathrm{d}C_p/\mathrm{d}(x/l)$. Using the measurements presented in figure 14, this parameter is of the order of 0.6 in the region of cloud cavitation. Hence, the increase in the re-entrant jet thickness due to the pressure gradient and given by (A 8), $\delta/d = \frac{1}{4}\mathrm{d}C_p/\mathrm{d}(x/l)$, is about 15%. This value is much larger than the thickness of the re-entrant jet in the absence of pressure gradient which was estimated to be a few percent only. These estimates confirm the major role played by the pressure gradient in the re-entrant jet, reinforcing substantially its thickness. Adding both values, we get a final estimate of the re-entrant jet thickness, taking into account the effect of the adverse pressure gradient, of about 18%. Although the present modelling of the effect of the pressure gradient is very crude, this calculated order of magnitude is in agreement with the measurements which were shown to lie between 15% and 35%.

6. Frequency content of the instability

From visualizations under stroboscopic lighting, it is possible to measure the characteristic frequency of cloud cavitation. This technique is easy to handle when

the shedding is very regular but is more and more unreliable as the limits of the periodic domain are approached. So, it was decided to carry out pressure fluctuation measurements and to make a more objective analysis of the frequency content of the instability from a spectral analysis of the signal.

As mentioned in § 2, a series of pressure transducers, flush mounted at various locations along the lower plate, was used. In the present work, we focus our analysis on the low-frequency domain. The high-frequency content has already been analysed by Reisman, Wang & Brennen (1998). Our simultaneous recording of the pressure signals at different locations together with the visualization of the cavity flow confirm their observation that two kinds of pressure pulses can be identified. The coherent collapse of the large-scale clouds, when they are convected to a region of high pressure, generates an instantaneous overpressure which is simultaneously detected by all the pressure transducers located in the collapsing zone. Unlike such *global* events, as named by Reisman *et al.*, *local* events were also observed. They are randomly distributed and correspond to the passing of a front of strong variation in the void fraction on the sensitive surface of the pressure transducer; they are interpreted as shock waves in the bubbly mixture by Reisman *et al.*

Returning to the low-frequency content of the pressure fluctuations, we observe that, in the regime of cloud cavitation, the pressure naturally oscillates at a frequency tuned to the shedding frequency. The pressure is minimum when cavitation covers the transducer. It reaches its maximum during the growing phase of the leading-edge cavity, when the cavity closure, which tends to be a stagnation point and so a region of high pressure, crosses the sensitive surface.

A spectral analysis of the pressure fluctuations was done for various operating conditions and in particular for different values of the cavity length. To minimize the influence of the location of the transducer in relation to the cavity closure, the cavitation parameter was systematically adjusted so that the cavity always closes on a given pressure transducer. The measurements were done using the pressure transducer located at the apparent cavity termination. For each cavity length considered here several step heights were considered, from 50 mm to 150 mm in steps of 25 mm, and a spectrum was obtained for each of them. All the spectra corresponding to the various step heights are juxtaposed to get the maps shown on figure 19.

The cloud shedding frequency is easily identified on all these maps. It corresponds to a Strouhal number close to 0.2 whatever the operating conditions may be, provided the Strouhal number is computed on the maximum cavity length. The lower and upper limiting values of the step height for which the peak in the spectra vanishes are in agreement with the mapping of the cloud cavitation instability presented on figure 8. The first harmonic which corresponds to a Strouhal number of about 0.4 is more visible for longer cavities or for less confined flows.

In addition to this fundamental frequency, another maximum is visible on the spectrum at low frequency, for long enough cavities, which is the signature of another type of cavitation instability. We already noted in § 3 (figure 8*a*) that, for long enough cavities, the cloud cavitation instability is replaced by a surge instability, characterized by an oscillation at a low frequency of the cavity length without any re-entrant jet. This instability is responsible for the maximum in the spectra observed on figures 19(*d*) and 19(*e*) at a frequency of about 3 Hz. Both instabilities occur simultaneously without any apparent interference between them.

When the length of the cavity increases, the cavity closes in a region of lower and lower pressure gradient because the adverse pressure gradient decreases very significantly downstream. From the strong correlation proved in the present work

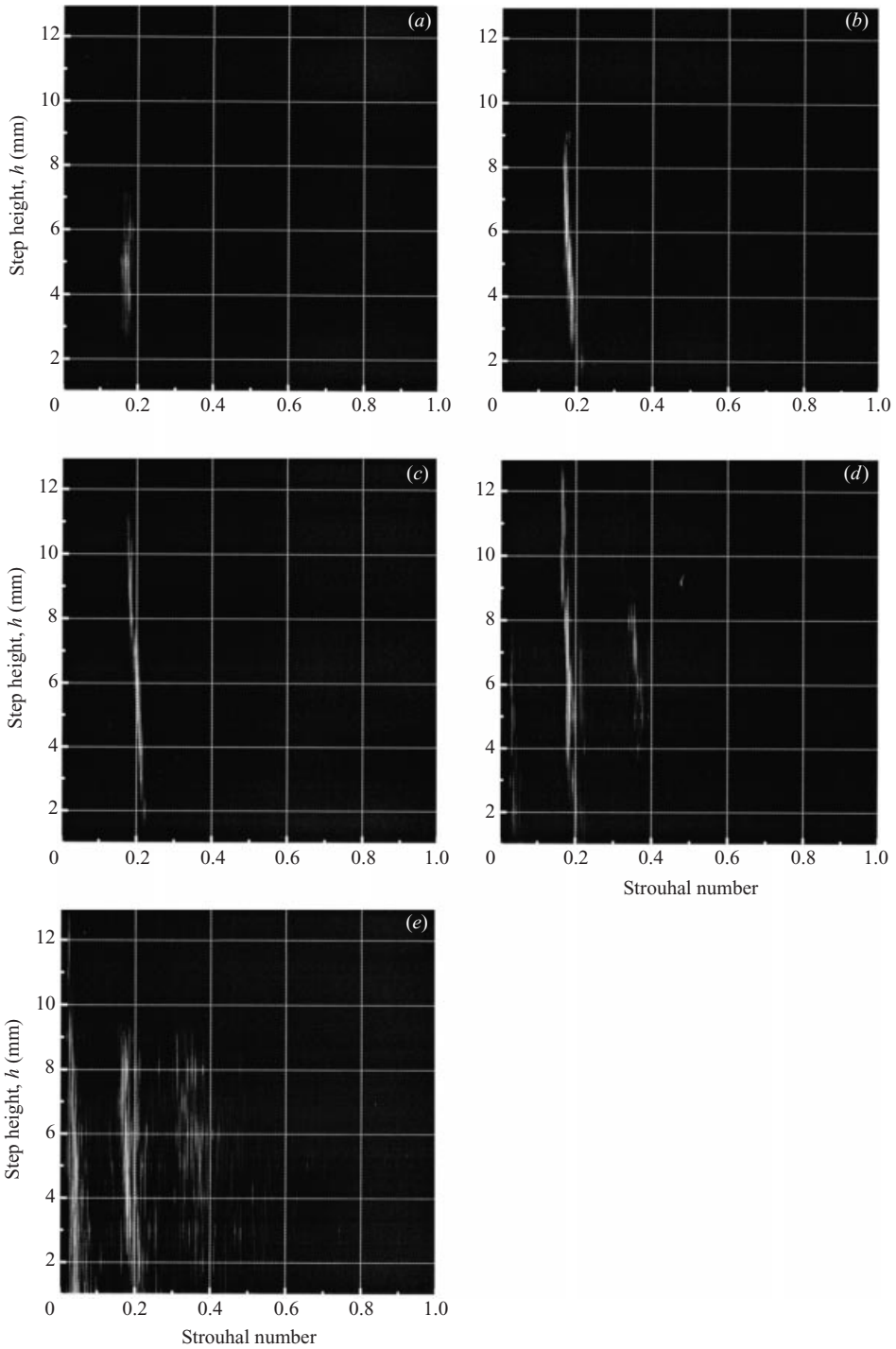

FIGURE 19. Spectra of the pressure transducer fluctuations for various operating conditions. The spectra obtained for various step heights are juxtaposed. Flow velocity 11.6 m s^{-1}, confinement height 20 mm, angle of attack 4.2°. Each diagram corresponds to a given cavity length: (*a*) 50 mm, (*b*) 75 mm, (*c*) 100 mm, (*d*) 125 mm, (*e*) 150 mm.

between the re-entrant jet instability and the adverse pressure gradient, it follows that the re-entrant jet instability progressively vanishes as the length of the cavity increases. The absence of significant pressure gradient for long cavities is the reason (1) for the disappearance of the re-entrant jet instability but also (ii) for the onset of the surge instability. If the pressure distribution is relatively flat in the closure region, the cavity can undergo significant oscillations in length even though the downstream pressure changes only very slightly. It is the case of extreme sensitivity to external fluctuations already discussed in the introduction which can lead to a surge-type instability because of the coupling of the dynamics of the cavity to the rest of the system.

7. Conclusion: towards the prediction of the dynamic behaviour of a partial cavity

From the present study, the dynamic behaviour of a partial cavity can be predicted as follows. The first key parameter to be considered is the pressure gradient. If the adverse pressure gradient at cavity closure is high enough, a re-entrant jet will develop at the back of the cavity. Then, two different patterns are possible according to the cavity thickness, which is the second key parameter. For thick enough cavities, the re-entrant jet does not interact significantly with the cavity interface as it moves upstream. The interaction is limited almost to the instant at which the re-entrant jet reaches the cavity leading edge and cuts the interface. A cavitation cloud is formed, and then the cavity grows again. This is the classical cloud cavitation instability.

If the cavity thickness is comparable to the re-entrant jet thickness, a strong interaction exists between the cavity interface and the re-entrant jet throughout its upstream movement. The vapour in the cavity splits into many small structures all along the re-entrant jet progression. The cavity appears rather like a two-phase mixture of approximately constant length. Although the cavity length does not oscillate, the dynamics of the re-entrant jet is still periodic.

On the other hand, if the adverse pressure gradient at closure is small or non-existent, the re-entrant jet and its subsequent instability cannot develop. The cavity can be considered as *open*. Unlike the case of cloud cavitation, the entrainment of vapour in the wake is more continuous. The relatively flat distribution of pressure around closure means that the cavity can easily lengthen, without significant resistance. Hence, small pressure disturbances originating in other components of the hydraulic system can trigger significant oscillations of the cavity length, which may, in their turn, react on the system. Unlike the case of the re-entrant jet instability, the instability which can develop in this regime is not intrinsic but system dependent.

Although the present results remain qualitative, they can help in the understanding of the stability of partial cavitation in other configurations and particularly in the practical case of cavitating foils. Unlike the present experimental arrangement for which the two main parameters, the adverse pressure gradient and the cavity thickness, could be changed almost independently, the case of a cavitating hydrofoil is more complicated as both parameters are mainly controlled by a single one, the angle of attack.

The pressure distribution on the suction side of a fully wetted foil is schematically given in figure 20. Although it may significantly differ from a foil section to another, two main zones can be distinguished. On the upstream part of the foil, say in the first half of the chord length, a region of high adverse pressure gradient exists as soon as

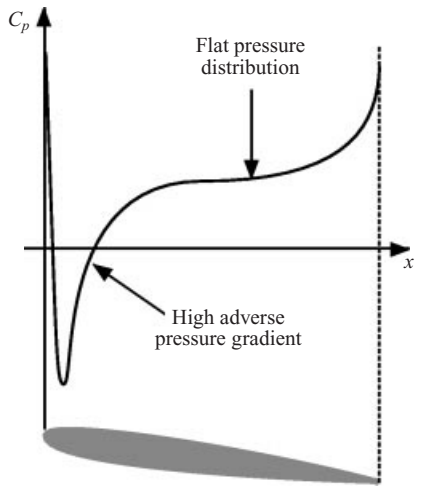

FIGURE 20. Typical pressure distribution on the suction side of a hydrofoil.

the angle of attack differs from 0. Downstream, the pressure distribution is relatively flat; approximately the second half of the chord length is a region of small pressure gradient.

Considering the results of the present study, it can be conjectured that the re-entrant jet instability can affect only small enough partial cavities, roughly shorter than half the chord length. Hence cavity auto-oscillations and subsequent cloud cavitation are expected to develop for such relatively short partial cavities. This point is in agreement with previous experiments on a hydrofoil (Le *et al.* 1993*a*) which showed that the auto-oscillation domain is roughly centred around the isocavity length $l/c = 0.5$. The same work also showed that smaller partial cavities do not experience auto-oscillation. Regarding the present results, this observation can be interpreted as an insufficient cavity thickness preventing the formation of large-scale clouds. To get the re-entrant jet instability on a hydrofoil, two conditions must be satisfied:

(i) the adverse pressure gradient must be large enough, which requires that the cavity length is not too long;

(ii) the cavity must not be too thin, which roughly imposes a minimum cavity length.

These arguments allow us to interpret qualitatively the limits of the domain of re-entrant jet instability observed on a hydrofoil by Le *et al.* (1993*a*) and shown on figure 3. However, the present qualitative analysis, based upon the non-cavitating pressure distribution, only gives general trends. A more advanced one should take into account (i) the feedback of the leading-edge cavity on the pressure distribution and (ii) the unsteady effects generated by the dynamic behaviour of the cavity.

This analysis also leads to the conjecture that the instability sometimes observed for long cavities, of around chord length, is probably not due to the development of a re-entrant jet but to a surge-type instability. As the pressure distribution at closure is flat for such long cavities, the conclusions drawn from the present work would lead to impute the instability between partial and super-cavitation to the extreme sensitivity of the cavity to external pressure fluctuations. Hence, it is likely that the characteristic frequency of such an instability is dependent upon the research facility, unlike the case of the re-entrant jet instability which leads to an almost constant Strouhal number which was found to lie between 0.2 and 0.4 by most

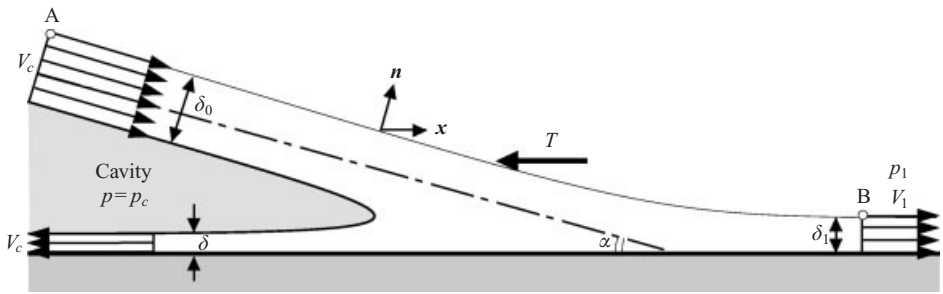

FIGURE 21. Sketch of the simplified model of the closure region of a cavity and corresponding notation.

investigators, whatever the operating conditions may be, the geometry tested or the research facility.

In conclusion, it appears of primary importance to know (i) the adverse pressure gradient at cavity closure and (ii) the relative orders of magnitude of the thicknesses of the cavity and of the re-entrant jet to be able to estimate the unsteady behaviour of a partial cavity. From a practical viewpoint, the stabilization of a partial cavity by the pressure gradient is difficult as the cloud cavitation instability, which occurs at high enough adverse pressure gradient, is progressively replaced by a surge-type instability when the pressure gradient is reduced. Hence, the control of cloud cavitation is probably more efficient by direct control of the re-entrant jet, either its surface in contact with the solid wall by using roughness or small obstacles, or its interface with the cavity by promoting the development of small-scale instabilities and the interaction with the external cavity interface.

This work was supported by the French 'Direction Générale de l'Armement'. We particularly thank M. Daniel Auchere from our Institute for his essential help in the development of the ultrasonic technique of measurement of the re-entrant jet thickness.

Appendix. A physical model

The external flow over the cavity can be considered as a liquid jet of thickness δ_0 at upstream infinity which impinges the wall with an angle α (cf. figure 21). It divides into two flows, the re-entrant jet of thickness δ and the co-current flow of thickness δ_1. The impinging current and the re-entrant jet, which both flow along the cavity at constant pressure p_c, are assumed to have the same velocity V_c and the same pressure p_c at infinity. The downstream pressure p_1 is assumed larger than p_c because of an adverse pressure gradient, and the flow velocity at downstream infinity, V_1, is smaller than V_c. The velocity profiles in the jets are assumed uniform. The adverse pressure gradient is modelled by a global tangential force T applied to the upper boundary of the flow (cf. figure 21). Such a boundary does not actually exist but is introduced as a schematic representation of the flow. Steady conditions are assumed.

The model is based on the balances of mass and tangential momentum :

$$V_c\delta_0 = V_1\delta_1 + V_c\delta, \tag{A 1}$$

$$\rho V_c^2\delta_0\cos\alpha - \rho V_1^2\delta_1 + \rho V_c^2\delta = (p_1 - p_c)\delta_1 + T, \tag{A 2}$$

where the tangential force T is defined by:

$$T = \int_A^B (p - p_c)\boldsymbol{n} \cdot \boldsymbol{x}\, \mathrm{d}l. \tag{A 3}$$

By combining the two equations, it is possible to compute the thicknesses δ and δ_1, i.e. to know how the impinging jet divides. In particular, the re-entrant jet thickness is given by

$$\delta = \frac{1 - 2\gamma\cos\alpha + \gamma^2}{(1+\gamma)^2}\delta_0 + \frac{2\gamma}{(1+\gamma)^2}\frac{T}{\rho V_c^2}, \tag{A 4}$$

where

$$\gamma = \frac{V_1}{V_c} = \sqrt{1 - \frac{2(p_1 - p_c)}{\rho V_c^2}}. \tag{A 5}$$

This equation is linearized assuming that the pressure gradient is small enough, i.e.

$$\frac{p_1 - p_c}{\rho V_c^2} \ll 1. \tag{A 6}$$

After linearization, we get the following simplified equation for the re-entrant jet thickness:

$$\delta = \delta^* + \frac{T}{2\rho V_c^2}, \tag{A 7}$$

where $\delta^* = \delta_0 \sin^2(\alpha/2)$ is the re-entrant jet thickness without a pressure gradient ($T = 0$).

The global tangential force T is here expressed in terms of the pressure gradient from a dimensional analysis. From (A 3) we have $T = O[(p_1 - p_c) l \sin\alpha]$ where l is the cavity length. The quantity $l\sin\alpha$ gives the order of magnitude of the cavity thickness, d. Hence, we have $T \approx (p_1 - p_c)\, d$. The pressure gradient $\mathrm{d}p/\mathrm{d}x$ is of order $(p_1 - p_c)/l$, so that we have $T \approx (\mathrm{d}p/\mathrm{d}x) l d$.

Returning to (A 7), the thickness of the re-entrant jet is given finally by

$$\delta \approx \delta^* + \frac{1}{4}\frac{\mathrm{d}C_p}{\mathrm{d}(x/l)}\, d \tag{A 8}$$

where C_p is the pressure coefficient defined here by $C_p = (p - p_{reference})/\frac{1}{2}\rho V_c^2$.

Equation (A 8) requires obtaining the thickness of the re-entrant jet without any pressure gradient, δ^*. Its order of magnitude can be obtained from a nonlinear calculation of the cavity flow behind a step in a semi-infinite medium. The analytical shape of the cavity is given by Michel (1978) (see also Laali & Michel 1984 for a similar problem):

$$\left.\begin{aligned} x(r) &= \frac{\lambda}{\pi}\left[\frac{1 - 2\lambda + 2\lambda^2}{\lambda^2} r + \ln(1 - r)\right], \\ y(r) &= -(1 - \lambda)\left[1 - \frac{1}{\pi}\cos^{-1}(2r - 1) - \frac{2}{\pi}\sqrt{r(1 - r)}\right], \end{aligned}\right\} \tag{A 9}$$

where r is a mathematical parameter varying between $r = 0$ at the detachment point and $r = 1$ at the infinity end of the re-entrant jet. The method used to compute the free surface of the cavity is classical and based upon standard techniques of conformal mapping (see e.g. Milne-Thomson 1960). The quantity λ is the thickness of the re-entrant jet non-dimensionalized by the step height and depends upon the

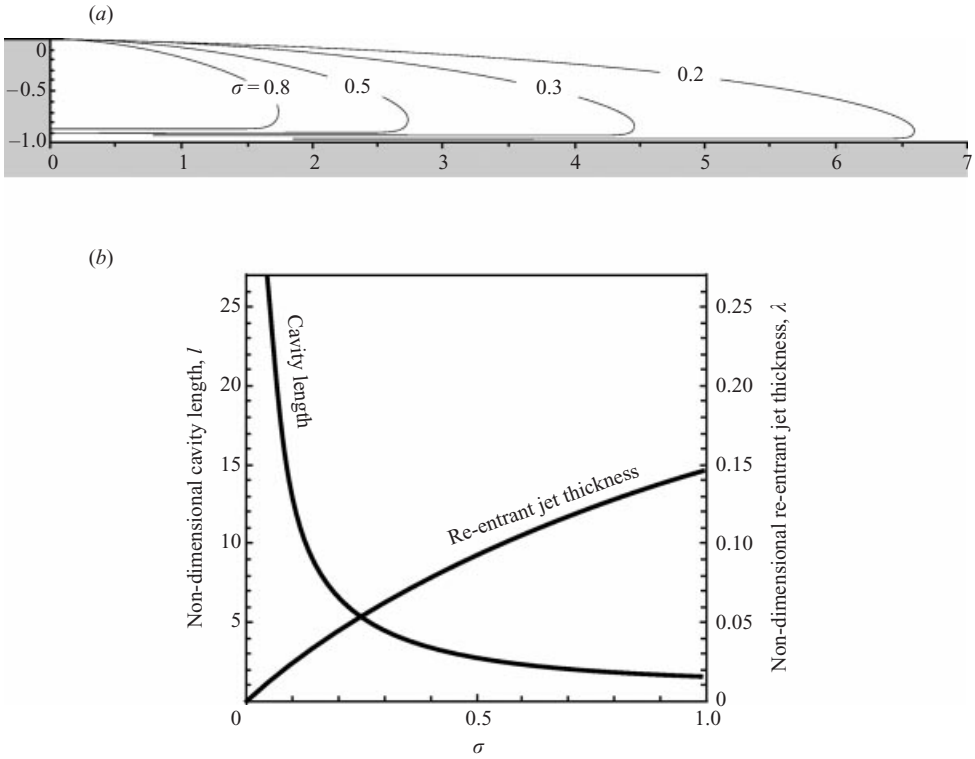

FIGURE 22. Nonlinear analytical computation of a cavitating step (Michel 1978) (*a*) Geometry of the cavity and of the re-entrant jet at various cavitation numbers. (*b*) Variations of the cavity length and of the re-entrant jet thickness with the cavitation number.

cavitation number σ:

$$\lambda = \frac{1}{2}\left[1 - \frac{1}{\sqrt{1+\sigma}}\right]. \tag{A 10}$$

The cavity length non-dimensionalized by the step height, l, is given by

$$l = \frac{\lambda}{\pi}\left[\frac{(1-\lambda)^2}{\lambda^2} + \ln\frac{\lambda^2}{1-2\lambda+2\lambda^2}\right]. \tag{A 11}$$

The shape of the cavity together with the variations of the cavity length and of the re-entrant jet thickness with the cavitation number are given in figure 22.

REFERENCES

AVELLAN, F. & DUPONT, P. 1988 Etude du sillage d'une poche de cavitation partielle se développant sur un profil hydraulique bi-dimensionnel. *La Houille Blanche* **7/8**, 507–515.

BOEHM, R., HOFMANN, M., LUDWIG, G. & STOFFEL, B. 1998 Investigations on possibilities to control the erosive cavitation aggressiveness by hydrodynamic effects. *Proc. Third Intl Symp. on Cavitation* (ed. J. M. Michel & H. Kato), Vol. 2, pp. 121–127.

BOEHM, R., STOFFEL, B. & LUDWIG, G. 1997 Investigations on the unsteady behaviour of cavitation and the corresponding pressure field. *La Houille Blanche* **4/5**, 84–88.

BRENNEN, C. E. 1995 *Cavitation and Bubble Dynamics*. Oxford University Press.

BRIANÇON-MARJOLLET, L. & MICHEL, J. M. 1990 The hydrodynamic tunnel of I.M.G.: former and recent equipments. *Trans. ASME: J. Fluids Engng* **112**, 338–342.

Ceccio, S. L. & George, D. L. 1996 A review of electrical impedance techniques for the measurement of multiphase flows. *Trans. ASME: J. Fluids Engng* **118**, 391–399.

Dang, J. & Kuiper, G. 1998 Re-entrant jet modelling of partial cavity flow on two-dimensional hydrofoils. *Proc. Third Intl Symp. on Cavitation* (ed. J. M. Michel & H. Kato), Vol. 2, pp. 233–242.

Dang, J. & Kuiper, G. 1999*a* Re-entrant jet modelling of partial cavity flow on two-dimensional hydrofoils. *Trans. ASME: J. Fluids Engng* **121**, 773–780.

Dang, J. & Kuiper, G. 1999*b* Re-entrant jet modelling of partial cavity flow on three-dimensional hydrofoils. *Trans. ASME: J. Fluids Engng* **121**, 781–787.

Dieval, L. 1999 Simulation des écoulements cavitants par poche par une méthode de suivi d'interface. PhD thesis, University of Aix-Marseille II, France.

Dieval, L., Arnaud, A. & Marcer, R. 1998 Numerical modeling of unsteady cavitating flows by a VOF method. *Proc. Third Intl Symp. on Cavitation* (ed. J. M. Michel & H. Kato), Vol. 2, pp. 243–248.

Driver, D. M. & Seegmiller, H. L. 1985 Features of a reattaching turbulent shear layer in divergent channel flow. *AIAA J* **23**, 163–171.

Dupont, P. 1993 Etude de la dynamique d'une poche de cavitation partielle en vue de la prédiction de l'érosion dans les turbomachines hydrauliques. PhD thesis, Ecole Polytechnique Fédérale de Lausanne, Switzerland.

Duttweiler, M. E. & Brennen, C. E. 1998 Partial cavity instabilities. *Proc. US-Japan Seminar: Abnormal Flow Phenomena in Turbomachines, Nov. 1–6, Osaka, Japan* (ed. Y. Tsujimoto & J. Katz).

Eaton, J. K. & Johnston, J. P. 1981 A review of research on subsonic turbulent flow reattachment. *AIAA J.* **19**, 1093–1100.

Furness, R. A. & Hutton, S. P. 1975 Experimental and theoretical studies of two-dimensional fixed-type cavities. *Trans. ASME: J. Fluids Engng* **97**, 515–522.

George, D. L., Iyer, C. O. & Ceccio, S. L. 2000 Measurement of the bubbly flow beneath partial attached cavities using electrical impedance probes. *Trans. ASME: J. Fluids Engng* **122**, 151–155.

Hashimoto, T., Yoshida, M., Watanabe, M., Kamijo, K. & Tsujimoto, Y. 1996 Experimental study on rotating cavitation of rocket propellant pump inducers. *32nd AIAA/ASME/SAE/ASEE Joint Propulsion Conf. July 1–3 1996, Lake Buena Vista, FL.*

Jovic, S. & Driver, D. 1995 Reynolds number effect on the skin friction in separated flows behind a backward-facing step. *Exps. Fluids* **18**, 464–467.

Kawanami, Y., Kato, H. & Yamaguchi, H. 1998 Three-dimensional characteristics of the cavities formed on a two-dimensional hydrofoil. *Proc. Third Intl Symp. on Cavitation* (ed. J. M. Michel & H. Kato), Vol. 1, pp. 191–196.

Kawanami, Y., Kato, H., Yamaguchi, H., Tagaya, Y. & Tanimura, M. 1997 Mechanism and control of cloud cavitation. *Trans. ASME: J. Fluids Engng* **119**, 788–795.

Kim, J., Kline, S. J. & Johnston, J. P. 1980 Investigation of a reattaching shear layer: flow over a backward-facing step. *Trans. ASME: J. Fluids Engng* **102**, 302–308.

Knapp, R. T., Daily, J. W. & Hammit, F. G. 1970 *Cavitation.* McGraw-Hill.

Kubota, A. 1988 Numerical studies of unsteady cavitation on a hydrofoil by a bubble two-phase flow model. PhD thesis, University of Tokyo, Japan.

Kubota, A., Kato, H. & Yamaguchi, H. 1992 A new modelling of cavitating flows: a numerical study of unsteady cavitation on a hydrofoil section. *J. Fluid Mech.* **240**, 59–96.

Kubota, A., Kato, H., Yamaguchi, H. & Maeda, M. 1989 Unsteady structure measurement of cloud cavitation on a foil section using conditional sampling technique. *Trans. ASME: J. Fluids Engng* **111**, 204–210.

Laali, A. R. & Michel, J. M. 1984 Air entrainment in ventilated cavities: case of the fully developed half-cavity. *Trans. ASME: J. Fluids Engng* **106**, 327–335.

Laberteaux, K. R. & Ceccio, S. L. 1998 Flow in the closure region of closed partial attached cavitation. *Proc. Second Intl Symp. on Cavitation* (ed. J. M. Michel & H. Kato), Vol. 1, pp. 197–202.

Laberteaux, K. R. & Ceccio, S. L. 1998 Partial attached cavitation on two- and three-dimensional hydrofoils. *Proc. 22nd ONR Symp. on Naval Hydrodynamics, Washington DC.*

de Lange, D. F. 1996 Observation and modelling of cloud formation behind a sheet cavity. PhD thesis, University of Twente, The Netherlands.

de Lange, D. F., Bruin, G. J. de & Wijngaarden, L. van 1994 On the mechanism of cloud cavitation – Experiment and modelling. *Proc. Second Intl Symp. on Cavitation* (ed. H. Kato), pp. 45–49.

Le, Q., Franc, J. P. & Michel, J. M. 1993*a* Partial cavities: global behaviour and mean pressure distribution. *Trans. ASME: J. Fluids Engng* **115**, 243–248.

Le, Q., Franc, J. P. & Michel, J. M. 1993*b* Partial cavities: pressure pulse distribution around cavity closure. *Trans. ASME: J. Fluids Engng* **115**, 249–254.

Michel, J. M. 1978 Demi-cavité formée entre une paroi solide et un jet plan de liquide quasi parallèles: approche théorique. *DRME Rep. 77/352 N° 4.*

Milne-Thomson, L. M. 1960 *Theoretical hydrodynamics.* MacMillan.

Pham, T. M., Larrarte, F. & Fruman, D. H. 1998 Investigation of unstable cloud cavitation. *Proc. Third Intl Symp. on Cavitation* (ed. J. M. Michel & H. Kato), Vol. 1, pp. 215–220.

Reisman, G. E., Wang, Y.-C. & Brennen, C. E. 1998 Observations of shock waves in cloud cavitation. *J. Fluid Mech.* **355**, 255–283.

Reboud, J. L. & Delannoy, Y. 1994 Two-phase flow modelling of unsteady cavitation. *Proc. Second Intl Symp. on Cavitation* (ed. H. Kato), pp. 39–44.

Reboud, J. L., Stutz, B. & Coutier, O. 1998 Two-phase flow structure of cavitation: experiment and modelling of unsteady effects. *Proc. Second Intl Symp. on Cavitation* (ed. J. M. Michel & H. Kato), Vol. 1, pp. 203–208.

Song, C. C. S. & He, J. 1998 Numerical simulation of cavitating flows by single-phase flow approach. *Proc. Third Intl Symp. on Cavitation* (ed. J. M. Michel & H. Kato), Vol. 2, pp. 295–300.

Stutz, B. & Reboud, J. L. 1997 Experiments on unsteady cavitation. *Exps Fluids* **22**, 191–198.

Tsujimoto, Y. 1995 Rotating cavitation: knowns and unknowns. *Proc. 1995 ASME/JSME Fluids Engng Div. Summer Meeting.*

Wade, R. B. & Acosta, A. J. 1966 Experimental observations on the flow past a plano-convex hydrofoil. *Trans. ASME: J. Basic Engng* **87**, 273–283.

Watanabe, S., Sato, K., Tsujimoto, Y., & Kamijo, K. 1999 Analysis of rotating cavitation in a finite pitch cascade using a closed cavity model and a singularity method. *Trans. ASME: J. Fluids Engng* **121**, 834–840.

Watanabe, S., Tsujimoto, Y., Franc, J. P. & Michel, J. M. 1998 Linear analyses of cavitation instabilities. *Proc. Third Intl Symp. on Cavitation* (ed. J. M. Michel & H. Kato), Vol. 1, pp. 347–352.

Yamaguchi, H., Kato, H., Kamijo, A. & Maeda, M. 1990 Development of a laser holography system for the measurement of cavitation bubble clusters. *ASME 1990 Cavitation and Multiphase Flow Forum.*